European Journal of Medicinal Chemistry 124 (2016) 82–102

Contents lists available at ScienceDirect

European Journal of Medicinal Chemistry

journal homepage: http://www.elsevier.com/locate/ejmech

Research paper

New insights into selective PDE4D inhibitors: 3-(Cyclopentyloxy)-4-methoxybenzaldehyde O-(2-(2,6-dimethylmorpholino)-2-oxoethyl) oxime (GEBR-7b) structural development and promising activities to restore memory impairment

Chiara Brullo [a, 1], Roberta Ricciarelli [b, 1], Jos Prickaerts [c, 1], Ottavio Arancio [d, 1], Matteo Massa [a], Chiara Rotolo [a], Alessia Romussi [a], Claudia Rebosio [e], Barbara Marengo [b], Maria Adelaide Pronzato [b], Britt T.J. van Hagen [c], Nick P. van Goethem [c], Pasqualina D'Ursi [f], Alessandro Orro [f], Luciano Milanesi [f], Sara Guariento [a], Elena Cichero [a], Paola Fossa [a], Ernesto Fedele [e, g, 2], Olga Bruno [a, *, 2]

[a] Department of Pharmacy, Section of Medicinal Chemistry, School of Medical and Pharmaceutical Sciences, University of Genoa, Viale Benedetto XV, 3, 16132 Genoa, Italy
[b] Department of Experimental Medicine, Section of General Pathology, School of Medical and Pharmaceutical Sciences, University of Genoa, Via L.B. Alberti, 2, 16132 Genoa, Italy
[c] Department of Psychiatry and Neuropsychology, School for Mental Health and Neuroscience (MHeNS), Maastricht University, Universiteitssingel 50, 6229 ER, Maastricht, The Netherlands
[d] Department of Pathology & Cell Biology, Taub Institute for Research on Alzheimer's Disease and the Aging Brain, Columbia University, New York, NY 10032, USA
[e] Department of Pharmacy, Section of Pharmacology and Toxicology, School of Medical and Pharmaceutical Sciences, University of Genoa, Viale Cembrano, 4, 16147 Genoa, Italy
[f] Institute for Biomedical Technologies and National Research Council (ITB-CNR), Via Fratelli Cervi 93, 20090 Segrate, MI, Italy
[g] Center of Excellence for Biomedical Research, University of Genoa, Viale Benedetto XV, 9, 16132 Genoa, Italy

ARTICLE INFO

Article history:
Received 21 June 2016
Received in revised form
9 August 2016
Accepted 10 August 2016
Available online 13 August 2016

Keywords:
PDE4D inhibitors
cAMP enhancers
Memory behavior test
Pharmacokinetic analyses
Molecular dynamics simulation
In silico ADMET properties

ABSTRACT

Phosphodiesterase type 4D (PDE4D) has been indicated as a promising target for treating neurodegenerative pathologies such as Alzheimer's Disease (AD). By preventing cAMP hydrolysis, PDE4 inhibitors (PDE4Is) increase the cAMP response element-binding protein (CREB) phosphorylation, synaptic plasticity and long-term memory formation. Pharmacological and behavioral studies on our hit GEBR-7b demonstrated that selective PDE4DIs could improve memory without causing emesis and sedation. The hit development led to new molecule series, herein reported, characterized by a catechol structure bonded to five member heterocycles. Molecular modeling studies highlighted the pivotal role of a polar alkyl chain in conferring selective enzyme interaction. Compound **8a** showed PDE4D3 selective inhibition and was able to increase intracellular cAMP levels in neuronal cells, as well as in the hippocampus of freely moving rats. Furthermore, **8a** was able to readily cross the blood-brain barrier and enhanced memory performance in mice without causing any emetic-like behavior. These data support the view that PDE4D is an adequate molecular target to restore memory deficits in different neuropathologies, including AD, and also indicate compound **8a** as a promising candidate for further preclinical development.

Abbreviations: AD, Alzheimer Disease; cAMP, cyclic adenosine monophosphate; CR3, conserved region 3; CREB, cAMP response element-binding protein; cGMP, cyclic guanosine monophosphate; COPD, chronic obstructive pulmonary disease; COSY, correlation spectroscopy; GPCRs, G protein coupled receptors; LTP, long term potentiation; MD, molecular dynamics simulations; PDE, phosphodiesterase; PDE4Is, PDE4 inhibitors; PKA, protein kinase A; SAR, structure-activity-relationship; UCR1 and UCR2, upstream conserved region 1 and 2.

* Corresponding author.
E-mail address: obruno@unige.it (O. Bruno).

[1] These authors contributed equally to this work.
[2] These authors also contributed equally to this work.

http://dx.doi.org/10.1016/j.ejmech.2016.08.018
0223-5234/

1. Introduction

Alzheimer's disease (AD) and other types of dementia involve today approximately 35 million people worldwide, a number expected to increase exponentially in the near future. The main AD symptoms consist of a progressive brain disorder leading to cognitive failure, neuropsychiatric alterations and memory loss.

The cAMP/PKA/CREB transcription is a key pathway in memory formation [1,2] and its impairment is thought to be involved in memory loss occurring during neurodegenerative diseases characterized by cognitive disorders [3,4]. Therefore, the impaired CREB signaling is now considered a possible alternative target for AD pharmacological treatment [5,6].

As the increase of cAMP is a key step in the CREB phosphorylation pathway, the intracellular levels of this second messenger are critical and tightly regulated by the adenylate cyclase synthesizing activity and type 4 phosphodiesterase (PDE4) enzyme, which is responsible for cAMP degradation to 5′-AMP. Accordingly, PDE4 inhibitors (PDE4Is) have been found to facilitate long term potentiation (LTP) and to improve memory function in a variety of cognitive tasks, both under physiological and pathological conditions [7–12].

Recent insights in this field, including the studies on the memory rescue ability of our lead GEBR-7b (**1**, Fig. 1) [13,14], showed that selective inhibition of the PDE4D isoform results in memory improvements without side effects (i.e. emesis and sedation), thus validating PDE4D as an important target for neurodegenerative pathologies such as AD [15,16].

Focusing on PDE4 family, 4 genes encoded for as many members (PDE4A-B-C-D) and 25 splice variants [17,18].

Although the four PDE4 isoforms (A, B, C and D) show a high sequence similarity (78%) in their catalytic domain, they can be distinguished on the basis of two regulatory domains (UCR1 and UCR2), inserted between the N-terminal portion and the catalytic domain, as well as the C terminal helix conserved region 3 (CR3). It has been reported that PDE4 long forms are functional dimers and that dimerization is mediated by UCR1 and UCR2 interactions [19,20]. On the other side, PDE4 lacking UCR1 (short forms) are monomers. Many studies have been recently focused on the role of UCR1-UCR2 oligomers and also of the C terminal helix conserved region 3 (CR3) as negative regulatory domains [21,15].

Crystal structures of PDE4B and PDE4D with fragments of UCR1, UCR2 and CR3, obtained by differently engineered constructs, have been recently solved in presence and absence of inhibitors [15,22]. Unfortunately, these structures do not fully recapitulate the dynamic process of the interaction between the UCR2/CR3 and the PDE4 active site. Consequently, any detailed consideration about the PDE4B/PDE4D selectivity will be addressed only when complete X-ray structures of these isoforms in complex with their inhibitors become available.

PDE4 inhibitors may be classified as “typical” or “atypical” based on whether they interact with the catalytic domain alone or also with the UCR2 domain [23]. Roflumilast and apremilast (Fig. 1), two recently approved drugs for the treatment of chronic obstructive pulmonary disease (COPD) and psoriatic arthritis, respectively, are “typical” site-directed competitive inhibitors that show preferential activity toward PDE4B and PDE4D isoforms [24,25]. On the contrary, rolipram (Fig. 1) may be classified as an “atypical non selective” inhibitor, being able to bind only the catalytic domain or to extend its interaction to UCR2. These different interactions may cause weak or strong rolipram binding and could explain the so-called low- and high-affinity-rolipram binding sites (LARBS and HARBS) [26]. More recently, Burgin and co-workers, by exploiting the Y/F difference between human PDE4B and PDE4D in the UCR2 domain, reported the atypical selective inhibitors D159404 and D-28 (Fig. 1) [15,27].

During the last ten years, we reported the synthesis of several series of small molecules bearing a catecholic moiety (typical of rolipram-related PDE4Is) and an amino function, linked to the aromatic portion by an iminoether chain. The chain length and its spatial direction have been investigated in order to obtain information about the selectivity toward the different PDE4 isoforms [28–31]. Among the numerous compounds, in addition to **1** also compound **2** (Fig. 1), characterized by a hydroxypropyl chain ending with a hydroxy-piperidine moiety, showed an interesting enzymatic profile. Indeed, it inhibited PDE4D3 with an IC_{50} value of

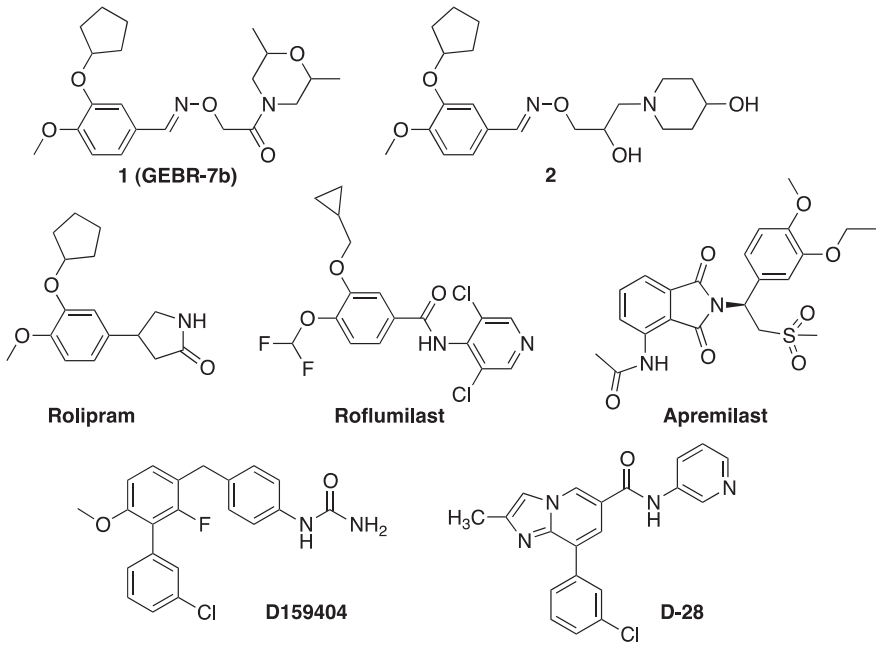

Fig. 1. Structures of compounds **1** (GEBR-7b), **2**, and some selective and non selective PDE4 inhibitors.

1.79 μM (versus 1.91 μM for **1**), and was almost completely inactive toward the PDE4A4, PDE4B2, PDE4C2 isoforms (% inhibition at 10 μM, less than 10%) [30]. This activity and selectivity improvement is justified by the fact that **2** is more polar than **1,** and makes three extra H-bonds with two water molecules and the backbone of residue N209, involving the OH group on the 4-hydroxypiperidine moiety, the OH positioned on the linker and the 4-hydroxypiperidine moiety nitrogen.

More recently, an accurate computational protocol, consisting of docking and molecular dynamics simulation (MD), has been applied to analyse in depth the interaction of compound **1,** and some of its derivatives, with the available crystal structure of the PDE4D catalytic site [32]. These computational results highlighted a new binding mode within the human PDE4D, in which the compounds were able to form a wide network of stable, direct and water-mediated H-bond interactions through their carbonyl or iminoether moieties, mainly in the nearby of Q369 and Y329 residues. Taken together, those MD simulation and our previous SAR considerations evidenced the pivotal role of the iminoether linker, and suggested to further investigate on this molecule portion to modulate activity and increase selectivity toward PDE4D isoforms.

Therefore, we designed new series of catechol-based derivatives where the iminoether function has been replaced by five membered heterocycles bearing the same alkyl chains used for previous compounds (Fig. 2). In particular, in compounds **3**–**4** and **5**–**7,** the iminoether function is inserted in an isoxazoline or isoxazole ring, respectively; in compounds **8**–**11,** the use of a pyrazole ring allowed the isosterism =N–O–/=N–N– and the contextual alkyl chain displacement in respect to the catechol portion. The heterocycle insertion, by reducing the molecules flexibility, gives fewer conformers and, therefore, should provide more information about pharmacophore features.

All synthesized compounds were screened on recombinant human PDE4D3 enzyme and, then, only active compounds (>50% inhibition) were tested on PDE4A4, PDE4B2 and PDE4C2 isoforms to assess their selectivity. An extensive in silico evaluation of pharmacokinetic and toxicity properties was performed to gain preliminary information on the most promising drug-like derivatives. Cytotoxic and genotoxic effects, and ability to increase cAMP in vitro were then evaluated for the most interesting compounds, selected on the basis of their enzymatic profile.

From the results of the in silico and in vitro studies, we chose compounds **8a** and **11b** for the in vivo pharmacokinetic analysis. Given its better pharmacokinetic profile, compound **8a** was further investigated in vivo to evaluate its ability to enhance cAMP levels in the hippocampus and to improve memory without side effects.

Finally, docking analyses and molecular dynamics (MD) simulation were performed on **4b** and **8a**, as representatives of structural diversity, to investigate the molecule-enzyme binding modes and support our SAR considerations.

2. Results and discussion

2.1. Chemistry

The starting building block 3-(cyclopentyloxy)-4-methoxybenzaldehyde **12** was obtained by isovanillin alkylation with bromocyclopentane, as reported in the literature [33]. The reactants chloroacetyl- or chloropropionylamines were prepared by condensation of chloroacetyl chloride or chloropropionyl chloride with the appropriate amines, according to our recently reported procedure [30].

For the synthesis of compounds **3**–**7,** the starting 3-(cyclopentyloxy)-4-methoxybenzaldehyde oxime **13** was obtained by reaction of the substituted benzaldehyde **12** with hydroxylamine in ethanol [29].

The oxime **13** was treated with *N*-chlorosuccinimide to obtain the 3-(cyclopentyloxy)-*N*-hydroxy-4-methoxybenzenecarboximidoyl chloride **14**, which was then cyclized with ethylacrilate, following a published procedure [34]. The intermediate dihydroisoxazole-5-carboxylate ethylester **15** was then treated with the appropriate amine to give compounds **3a**–**f** (Scheme 1).

Compounds **4a**–**g** were prepared by cyclization of the oxime-chloride **14** with 3-butenoic acid, obtaining the intermediate dihydroisoxazol-5-acetic acid **16** [34] that, in turn, was treated with the appropriate amine, in the presence of diphenylphosphorylazide (DPPA) (Scheme 1).

Also compounds **4a**,**b** have been prepared by an alternative convergent synthetic strategy, which involves the cyclization of oxime-chloride **14** with the suitable 1-amino-3-buten-1-ones **17a**,**b**. The latter were, in turn, prepared by a novel and simple one-pot reaction, starting from 3-butenoic acid, which was firstly transformed in the corresponding acyl chloride and subsequently condensed as a crude with the appropriate cycloamine (Scheme 1).

Compounds **5a**,**b** and **6a**,**b** were prepared by the procedure already reported in the literature for similar compounds [35]. The isoxazole intermediate **18** was obtained by a 1,3-dipolar addition of **14** with 3-butyn-2-ol. Then, the secondary alcohol group was oxidized with a mixture of acetic anhydride and dimethyl sulfoxide, yielding the corresponding keton **19** that was then α-brominated to derivative **20**. The bromoketone was treated with two equivalents of the appropriate cycloamine, obtaining the aminoketones **5a**,**b** that were immediately converted into their corresponding hydrochlorides to avoid decomposition. Then, the aminoalcohols **6a**,**b** were obtained by reducing **5a**,**b** with sodium borohydride and sodium methoxide in anhydrous methanol (Scheme 2). The cyclization of **14** with methylpropiolate ester gave the intermediate isoxazole ester **21** that, in turn, was treated with an excess of the suitable cycloamine to give compounds **7a**,**b** (Scheme 2).

In order to synthesize the pyrazole derivatives **8**–**11,** we first

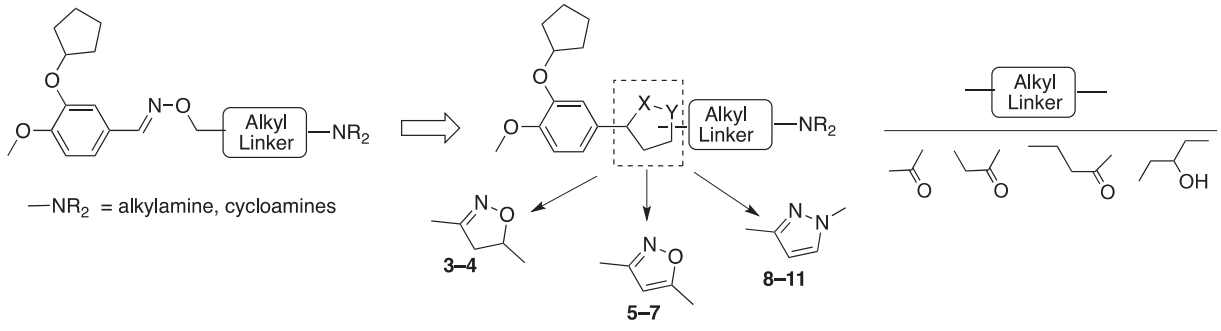

Fig. 2. Development of new catechol-based heterocyclic derivatives.

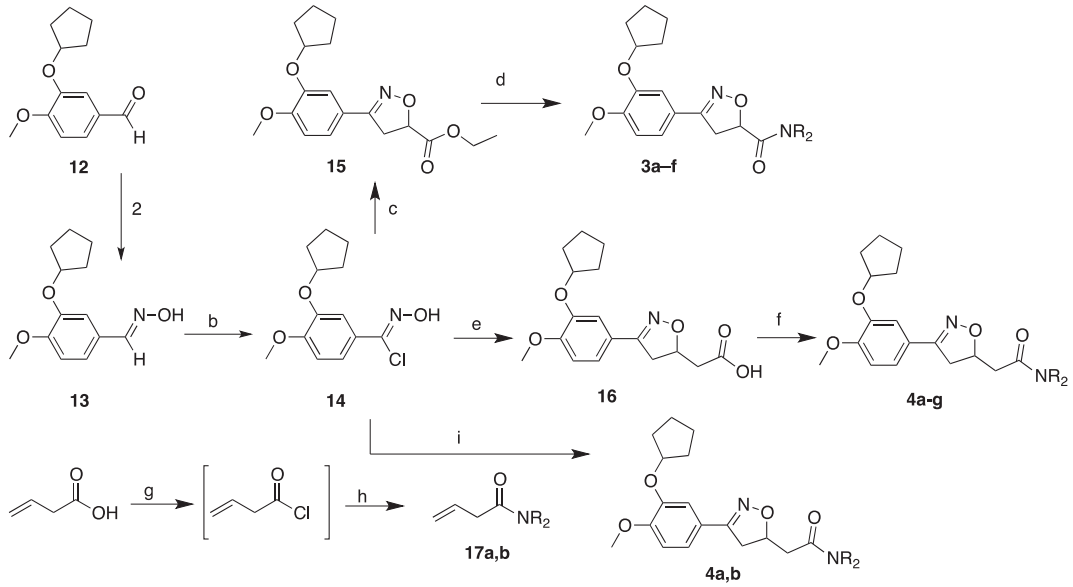

Scheme 1. Synthesis of compounds **3a**-**f**, **4a**-**g** and **17a**,**b**. Reagents and conditions: (a) $NH_2OH \cdot HCl$, $NaHCO_3$, H_2O/EtOH, rt, 4 h, 61%; (b) *N*-chlorosuccinimide, an. DMF, 40–50 °C, 1 h, 65%; (c) acrylic acid ethyl ester, DCE, TEA, 0 °C, nitrogen atmosphere, then 60 °C, 1 h, then rt, 48 h, 50%; (d) excess cycloamine or cycloamine in an. DMF, 60 °C, overnight, 22–85%; (e) 3-butenoic acid, DCE, TEA, added at 0 °C under nitrogen atmosphere, then 60 °C, 1 h, then rt, 48 h, 35%; (f) cycloamine, an. DMF, TEA, DPPA, 80 °C, 24 h, 21–70%; (g) thionyl chloride, 60 °C, 30 min; (h) cycloamine, an. THF, rt, 2 h, 67% (**17a**) or 72% (**17b**); (i) **17a** or **17b**, an. DMF, TEA, 0 °C under nitrogen atmosphere, then rt, 72 h, 41% (**4a**) or 40% (**4b**).

prepared the building block 3-[3-(cyclopentyloxy)-4-methoxyphenyl]-1*H*-pyrazole **22** by a one-pot 1,3-dipolar cycloaddition [36]. In details, the 3-(cyclopentyloxy)-4-methoxybenzaldehyde **12** was treated with *p*-toluenesulfonyl hydrazide, NaOH and 1-vinylimidazole in acetonitrile (Scheme 3).

The pyrazole intermediate **22** was then treated with an excess of epichlorohydrin in the presence of TEA. This reaction could lead to 1,5 and/or 1,3 di-substituted pyrazole isomers. The ^1H and ^{13}C NMR spectra analyses showed a 1,3-disubstituted pyrazole structure for the oxirane derivative (**23**), as reported in the experimental section.

The reaction of the above mentioned **23** with an excess of the suitable cycloamine gave compounds **8a**–**c** in good yields. The acetyl derivative **9a** was obtained from **8a** with acetic anhydride (Scheme 3).

The treatment of the above pyrazole derivative **22** with 4-(chloroacetyl)morpholine or 4-(chloroacetyl)-2,6-dimethylmorpholine, in the presence of triethylamine (TEA), led to the amide derivatives **10a**,**b** (Scheme 3).

The same procedure was used to obtain **11a**, starting from the pyrazole derivative **22** and 4-(3-chloropropanoyl)morpholine (Scheme 3). On the other hand, in order to obtain the analogue **11b**, the pyrazole **22** was treated with an excess of methyl 3-bromopropanoate, yielding the intermediate **24** that was then hydrolized to the corresponding acid **25**. The latter was treated with 2,6-dimethylmorpholine, in the presence of TEA and DPPA, to obtain the desired product **11b** (Scheme 3).

2.2. Enzymatic assays

A preliminary screen was performed by testing our compounds on recombinant human PDE4D3 activity, at the concentration of 10 μM in duplicate (Table 1), as previously reported [29–31]. To obtain information about the inhibitory potency on PDE4D3, the most active compounds (i.e. those showing inhibition >50%) have been further tested in the same assay at five different concentrations (5×10^{-8}–10^{-4} M) and IC_{50}s were determined by nonlinear regression analysis of the inhibition curve, using Hill equation curve fitting (Graph Pad Prism software) (Table 2).

In addition, we have also analysed their selectivity toward PDE4A4, PDE4B2 and PDE4C2 using the strategy of the single concentration (10 μM) assay (Table 2).

Most of newly synthesized compounds showed low activity toward PDE4D3 (inhibition less than 40%). In the case of the isoxazoline series, only compounds **4b**, **4d**, and **4g** showed a PDE4D3 inhibition higher than 50% with IC_{50} values of 5.58 μM, 1.22 μM and 1.11 μM, respectively. On the contrary, all derivatives of the series **3**, which are apparently the most similar to our lead **1**, were inactive. Assuming that the same interaction between the enzyme and the catechol scaffold, as well as the C=N–O–C– moiety, occurs for compounds **1**, **2**, **3** and **4**, it is likely that the inclusion of the latter group in the more planar and rigid ring is detrimental for the proper enzyme-interaction of the terminal amino group. This observation is strongly supported by the comparison between compounds **3b** (20% of inhibitory activity), **4b** (51% inhibition, IC_{50} 5.58 μM) and **1** (67% inhibition, IC_{50} 1.91 μM). On the other hand, although the activity of dimethylmorpholino and diethanolamino derivatives **4b** and **4g** was predictable on the basis of our previous SAR considerations (highlighting the essential role for oxygen atom in the chain end), the potency of the pyrrolidino derivative **4d**, as well as the inactivity of **4a** and **4c**, were unexpected and are difficult to explain. In addition, in this series, only **4b** resulted in PDE4D3 selective inhibition, while both **4d** and **4g** were significantly active also on PDE4A4 and PDE4B2 (inhibition higher than 50%).

In agreement with the above observations, also the more planar and rigid isoxazole derivatives **5**, **6**, and **7** were inactive. Moreover, the lack of activity for **5a** and **5b** matches the inactivity of the analogue open-chain aminoketone derivatives previously reported [30].

Among the pyrazole isoster derivatives, the most active ones were **8a**, **8b** and **11b** with IC_{50} values of 7.6 μM, 6.0 μM and 1.8 μM, respectively, while **11a** showed only 42% of PDE4D3 inhibition and **10a** and **10b** were inactive. Once again, only the molecules bearing the longest linker (e.g. **8** and **11**) may take the required amino terminal spatial arrangement. Interestingly, **9a**, the acetyl derivative of **8a**, showed very low activity, thus confirming that the hydroxypropyl chain needs a free –OH group to strongly interact

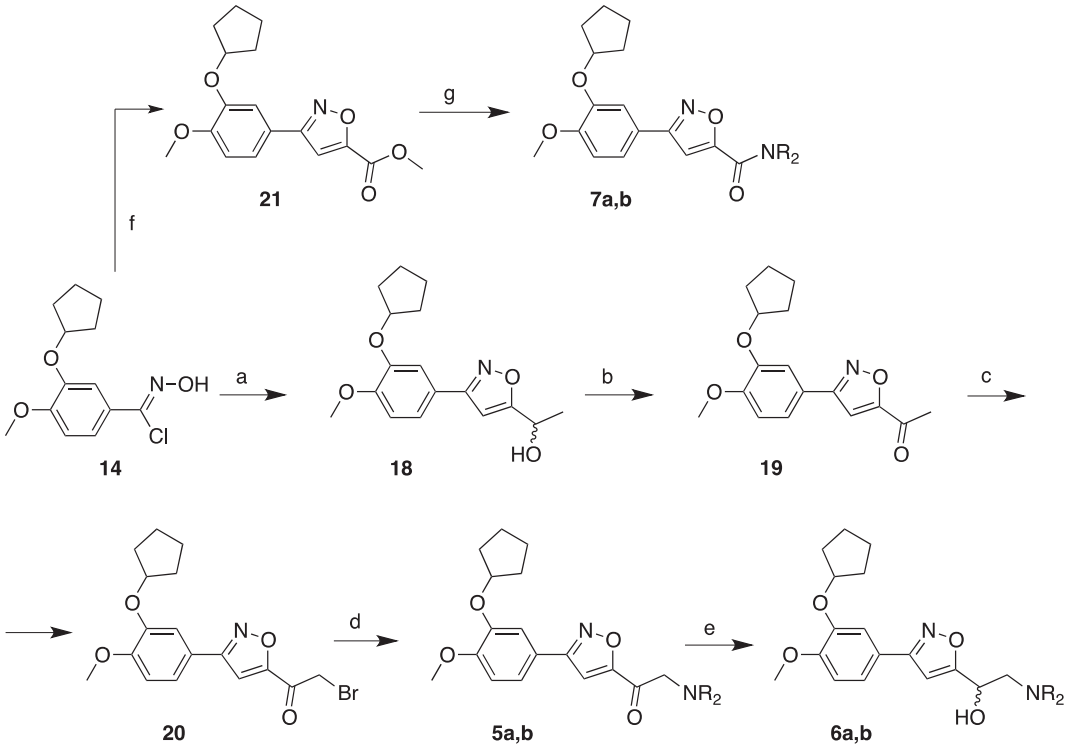

Scheme 2. Synthesis of compounds **5a**,**b**, **6a**,**b**, **7a**,**b**. Reagents and conditions: (a) 3-butyn-2-ol, an. toluene, TEA, 60 °C, 18 h, 60%; (b) acetic anhydride, DMSO, rt, 24 h, 80%; (c) glacial acetic acid, DCM, 50 °C, then bromine in DCM, 60–70 °C, 1 h, 60%; (d) cycloamine, DCM, −10 °C (for **5a**) or −30 °C (for **5b**), 5 min, then sat. HCl sol. in an. diethyl ether, 72% (**5a**) or 25% (**5b**); (e) $NaBH_4$, an. methanol, then sodium methoxide in an. methanol, rt, 4 h, 65% (**6a**) or 30% (**6b**); (f) methyl propiolate, an. toluene, TEA, 60 °C, 12 h, 33%; (g) cycloamine, 60 °C, 12 h, 53% (**7a**) or 69% (**7b**).

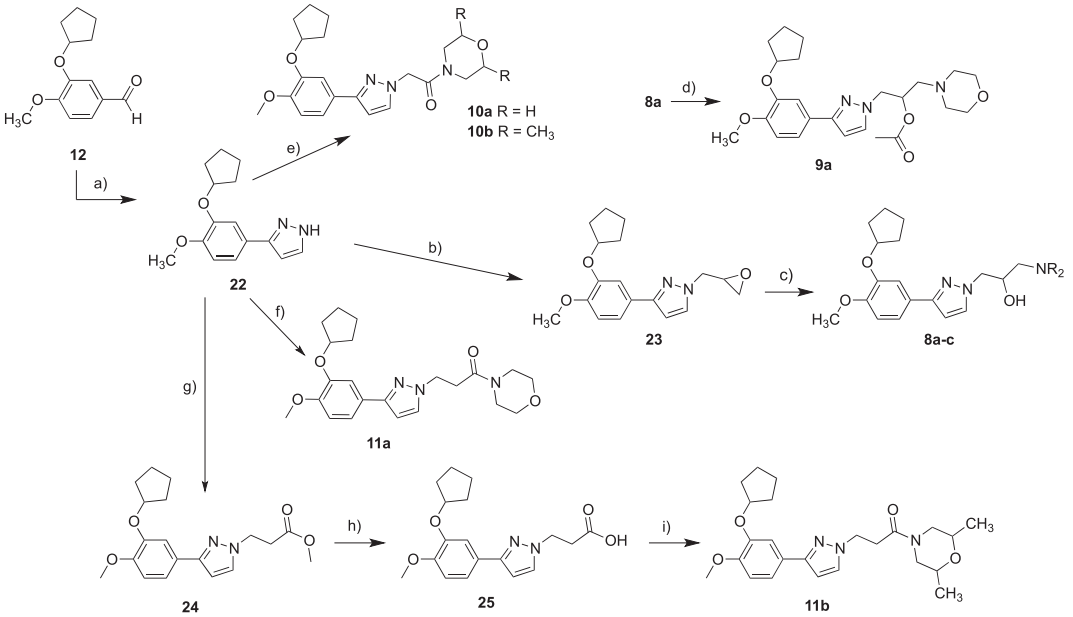

Scheme 3. Synthesis of compounds **8a**-**c**, **9a**, **10a**,**b** and **11a**,**b**. Reagents and conditions: (a) *p*-toluenesulfonyl hydrazide, an. CH_3CN, rt, 1 h, then 5 M NaOH and 1-vinylimidazole, 50 °C, 48 h, 65%; (b) epichlorohydrin, TEA, 70 °C, 3 h, 73%; (c) morpholine or 2,6-dimethylmorpholine excess, or 4-hydroxypiperidine in an. DMF, 50–60 °C, 18 h, 40–61%; (d) acetic anhydride, sodium acetate, 40–50 °C, 5 h, 52%; (e) chloroacetylmorpholine or chloroacetyl-2,6-dimethylmorpholine, TEA, an. DMF, 60 °C, 24 h, 53% (**8a)** or 58% (**8b**); (f) chloropropionylmorpholine, TEA, DMF an., 120 °C, 48 h, 38%; (g) methyl-3-bromopropionate, TEA, an. CH_3CN, 70 °C, 24 h, 67%; (h) NaOH, EtOH, 60 °C, 4 h, 74%; (i) 2,6-dimetylmorpholine, TEA, DPPA, an. DMF, 80 °C, 15 h, 71%.

with PDE4D. Quite surprisingly, however, is the total lack of activity of the 4-hydroxy-piperidine derivative **8c**, considering the close structural correlation with our previous potent and selective inhibitor **2**. Finally, among active compounds, **8a** and **11b** were the most selective PDE4D3 inhibitors.

In conclusion, the pyrazole series **8a**–**c** and **11a**,**b** showed the

Table 1
Molecular structure and inhibition activity of compounds 3a–f, 4a–g, 5a,b, 6a,b, 7a,b, 8a–c, 9a, 10a,b, 11a,b, 12a–c, 13a,c, and 14a–c toward PDE4D3[a].

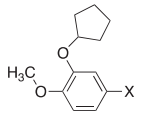

Compound	X	Y	NR_2	PDE4D3 % Inhib (10 μM)
3a	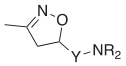	CO		21
3b	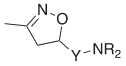	CO		29
3c	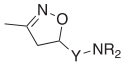	CO	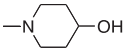	26
3d	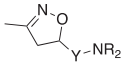	CO		15
3e	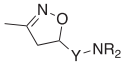	CO		8
3f	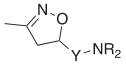	CO	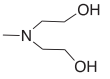	33
4a	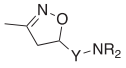	CH_2CO		29
4b	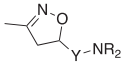	CH_2CO		51
4c	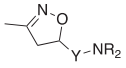	CH_2CO	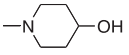	30
4d	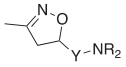	CH_2CO		57
4e	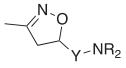	CH_2CO		40
4f	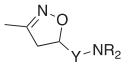	CH_2CO		23
4g	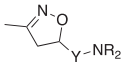	CH_2CO	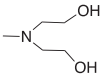	65
5a	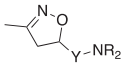	$COCH_2$		39
5b	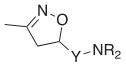	$COCH_2$		13
6a	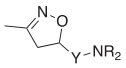	$CH(OH)CH_2$		38
6b	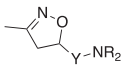	$CH(OH)CH_2$		15

(*continued on next page*)

Table 1 (*continued*)

Compound	X	Y	NR_2	PDE4D3 % Inhib (10 μM)
7a	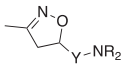	CO		41
7b	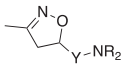	CO		35
8a	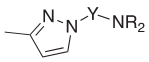	$CH_2CH(OH)CH_2$		68
8b	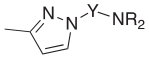	$CH_2CH(OH)CH_2$		78
8c	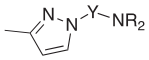	$CH_2CH(OH)CH_2$	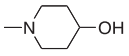	2
9a	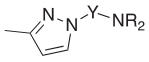	$CH_2CH(OCOCH_3)CH_2$		28
10a	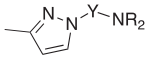	CH_2CO		27
10b	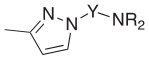	CH_2CO		23
11a	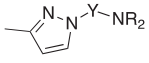	CH_2CH_2CO		42
11b	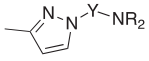	CH_2CH_2CO		53
1		CH_2CO		67
rolipram	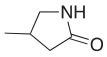	–	–	79

[a] Data are expressed as % of inhibition with respect to controls. All drugs have been tested in duplicate at the concentration of 10 μM. Compound **1** and rolipram have been used as reference compounds.

Table 2
Inhibition activity of compounds **4b,d,g, 8a,b** and **11b,** toward PDE4D3, PDE4A4, PDE4B2 and PDE4C2[a].

Compound	PDE4D3 % Inhib 10 μM (IC_{50} μM)	PDE4A4 % Inhib 10 μM	PDE4B2 % Inhib 10 μM	PDE4C2 % Inhib 10 μM
4b	51 (5.58)	45	27	23
4d	57 (1.22)	66	59	47
4g	65 (1.11)	69	67	40
8a	68 (7.6)	22	18	11
8b	78 (6.0)	52	53	45
11b	53 (1.8)	28	28	42
1[b]	67 (1.91)	34	23	25
Rolipram[b]	79 (0.09)	79	65	57

[a] Data are expressed as % inhibition with respect to controls. All drugs have been tested in duplicate at the concentration of 10 μM. Values for PDE4D3 inhibition are taken from Table 1. IC_{50} values for PDE4D3 are reported in parenthesis. Compound **1** and rolipram have been used as reference compounds.
[b] Data taken from Ref. [29].

most interesting enzymatic profile. Compound **11b** was the most potent on PDE4D3, whereas **8a** showed the highest selectivity (Tables 1 and 2).

2.3. Computational studies

2.3.1. Molecular dynamics and docking

A recent molecular dynamics simulation (MD) study was performed to analyse in depth the interaction of compound **1** with the

available crystal structure of the PDE4D catalytic site [32]. The results revealed a new binding mode of **1,** and some of its derivatives, within the human PDE4D, in which the compounds formed a wide and stable H-bonded network, mainly in the nearby of Q369 and Y329 residues, making direct and/or water-mediated H-bonds through their carbonyl and iminoether moieties.

On this basis, we found it interesting to investigate the binding mode of compounds **4b** and **8a**, where the iminoether function, emerged as an interesting binding feature in compound **1** and its derivatives, has been inserted in an isoxazoline ring or has been substituted by a pyrazole ring. In addition, **4b** and **8a** well represent the series with a high degree of molecular diversity bearing different linkers, that are an amide carbonyl (similarly to **1**) or a hydroxypropyl chain (similarly to **2**), respectively.

Starting from the most promising conformation obtained from the docking, we performed MD studies. For each MD simulation, the most represented complex conformation was evaluated. Compound **8a** conformation was stable, in agreement with the experimental data assessing its relevant inhibitory activity on PDE4D. Its occupancy of the binding site is different from that of compound **1** and is very similar to that of roflumilast (Figs. 3 and 4), being located more closely to the metal ions. Compound **8a** is anchored to the enzyme by several hydrogen bonds, from the extremities all along its structure, including the centre (Fig. 4, left).

In details, an H-bond involves one catechol oxygen and Q369, while the alcoholic oxygen of **8a**, the key features anchoring the molecule into the catalytic site, is engaged in two H-bonds, one with H160 and the other with a water molecule of the metal pocket. Furthermore, the morpholino nitrogen makes an H-bond with M273 backbone.

As concerns compound **4b**, it is worth noting that the substitution of the flexible chain of **1** with an unsaturated isoxazole ring determines the occupancy of the same binding area that we already described for **1** [32]. However, the spatial orientation, imposed to the chain and to the morpholino moiety by the unsaturated five-membered ring, forces **4b** to move in a region where the side chains of Q369 and Y329 are normally located. Consequently, in a sort of "domino effect", these two interactions are lost by the ligand

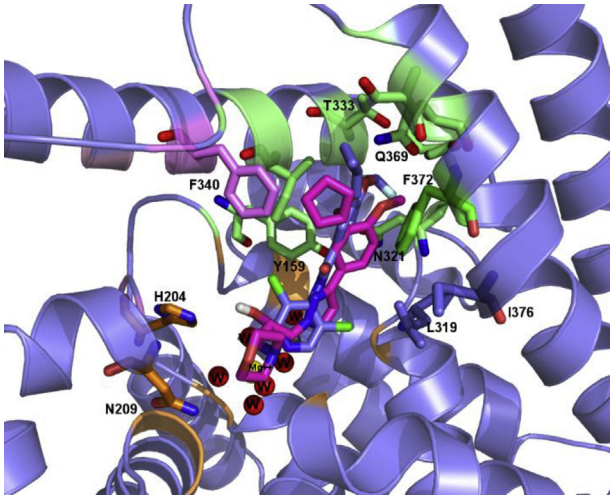

Fig. 3. The proposed binding of compound **8a** (magenta) in comparison with roflumilast (slate blue) into PDE4D active site. The main amino acid residues are shown in sticks, the enzyme is shown in cartoon diagram. The residues forming the metal binding, Q switch and P clamp and solvent filled side pockets displayed in cartoon diagram are coloured orange, pink and green respectively. Zinc and Magnesium ions and waters are represented as spheres. (For interpretation of the references to colour in this figure legend, the reader is referred to the web version of this article.)

(see Fig. 1 in Supporting Information). In details, **4b** does not perform the bi-dentate H-bond with Q369 since the spatial orientation of the carbonyl group forces Q369 side chain to turn differently, in order to avoid the clash. In addition, its morpholino ring displaces the water molecule close to Y329, thus the inhibitor loses that water mediated H-bond already observed for compound **1**. The ligand is anchored to the protein by two H-bonds: the amidic carbonyl binds T333 and the morpholino oxygen binds N321. An additional $\pi-\pi$ interaction with F372 completes the pattern (see Fig. 2 in Supporting Information).

These computational results are fully in agreement with the experimental data and highlight, once more, the importance of the iminoether linker to determine a high PDE4D inhibitory activity (compound **1**). On the other hand, also the alkyl linker plays a role on the inhibitor arrangement in the catalytic site, as highlighted by compound **4b** interactions. In addition, the isosterism =N–O–/= N–N given by the pyrazole ring seems to guarantee a good inhibitory activity on PDE4D also for compound **8a,** since the molecule retains a favourable spatial orientation of the chain and of the morpholino moiety into the catalytic pocket. Moreover, this study emphasises a very important role of the alcoholic function to address the rational design of new compounds and confirm the above SAR considerations. In fact, in the case of **8a**, its polarity strongly drives the molecule toward the metal pockets where several H-bonds stabilize the ligand. These interactions replace that with Y329, and make the complex of **8a** with the enzyme very stable.

2.3.2. In silico evaluation of pharmacokinetic properties

The computational prediction of descriptors related to absorption, distribution, metabolism, excretion and toxicity (ADMET) properties represents a useful in silico strategy accelerating the lead compound discovery process [37].

In this work,, a series of ADMET properties was calculated for the newly synthesized compounds **3b**, **8a**, **8b**, **11b**, **4b**, **4d** and **4g**, being the most active PDE4D3 inhibitors, and also for **1**, rolipram and roflumilast, as reference compounds. In particular, we evaluated the logarithmic ratio of the octanol-water partitioning coefficient (cLogP), the extent of blood-brain barrier permeation (LogBB), the rate of passive diffusion-permeability (LogPS), the human intestinal absorption (HIA), the volume of distribution (Vd), the role played by plasmatic protein binding (%PPB) and by the compound affinity toward the human serum albumin ($LogK_a^{HSA}$), and the overall estimation of oral bioavailability (%F).

In addition, a number of descriptors predictive of compound metabolism and toxicity were estimated, including the compound potential behavior as P-glycoprotein inhibitor/substrate, the ability to interact with the endocrine system or to act as a cytochrome P450 3A4 inhibitor/substrate, and the median lethal dose (LD_{50}) related to oral administration.

As shown in Table 3, all the compounds are characterized by a favourable profile in terms of lipophilicity, being the calculated cLogP below 5 (Lipinski rules), and also display the ability to be fully adsorbed by the human intestinal membrane (HIA). Notably, all derivatives show an adequate blood-brain barrier permeation, showing LogBB and/or LogPS values falling in the recommended ranges ($0 < LogBB < 1.5$; $-3 < LogPS < -1$.

The values of the calculated volume of distribution (Vd) and of the potential binding to plasma proteins (%PPB) seem acceptable and are within those displayed by rolipram and roflumilast. Finally, the newly synthesized compounds show a very favourable oral bioavailability profile (%F, column 8), especially being those of **8a** and **11b** higher than that of **1**.

According to the descriptors listed in Table 4, none of our PDE4D inhibitors should be substrate or inhibitor of the P-glycoprotein, or

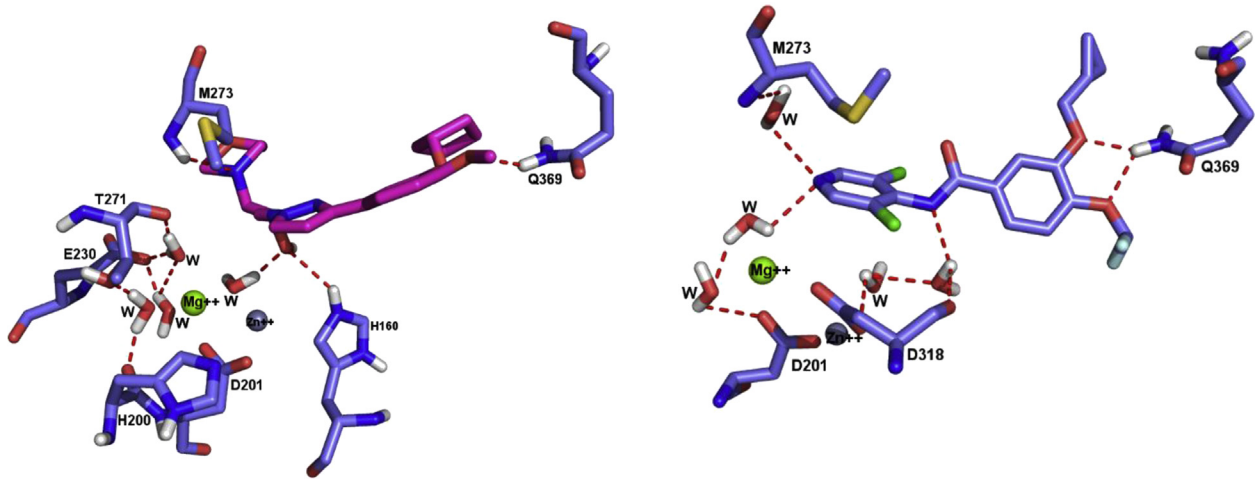

Fig. 4. The putative binding mode of compound **8a** (left) and roflumilast (right) within the PDE4D active site. Ligand carbon atoms are coloured in magenta and slate blue respectively, protein carbon atoms are coloured in slate blue. The main amino acid residues are shown in sticks. Zinc and Magnesium ions are represented as spheres and the H-bonds between each ligand and the active site amino acid are shown as dashed line. (For interpretation of the references to colour in this figure legend, the reader is referred to the web version of this article.)

Table 3
Calculated ADMET descriptors related to absorption and distribution properties.

Comp.	cLogP	LogBB[a]	LogPS[b]	HIA (%)[c]	Vd (l/kg)[d]	%PPB	$LogKa^{HSA}$	%F (oral)
1	3.45	0.76	−1.3	100	1.9	76	3.66	97.5
3b	3.79	0.94	−1.2	100	2.1	77	3.82	97.1
8a	2.54	0.25	−1.7	100	2.0	76	4.02	99.6
8b	3.75	0.48	−1.5	100	2.4	80	4.08	99.6
11b	3.26	0.32	−1.3	100	2.1	89	4.75	99.2
4b	2.98	0.48	−1.4	100	2.0	77	4.16	98.2
4d	2.73	0.35	−1.4	100	1.8	77	4.09	99.4
4g	1.23	−0.14	−2.5	100	1.4	66	3.37	99.6
Rolipram	1.72	0.07	−1.7	100	1.4	62.53	3.69	99.6
Roflumilast	3.42	−0.13	−1.3	100	2.0	96.67	4.20	42.2

[a] Extent of brain penetration based on ratio of total drug concentrations in tissue and plasma at steady-state conditions.
[b] Rate of brain penetration. PS represents Permeability-Surface area product and is derived from the kinetic equation of capillary transport.
[c] HIA represents the human intestinal absorption, expressed as percentage of the molecule able to pass through the intestinal membrane.
[d] Volume of Distribution (Vd) of the compound in the body.

be involved in toxicity events such as binding with the endocrine system. Indeed, all the compounds are characterized by acceptable LogRBA values, being lower than −3 within high reliability indices. Interestingly, none of our PDE4D inhibitors are able to inhibit CYP3A4, whereas they may be its substrates.

Finally, all compounds exhibit a favourable toxicity profile, being the estimated LD_{50} in the range of 640–1400 mg/kg for mouse after oral administration, values that are comparable with those calculated for rolipram and roflumilast.

2.4. In vitro genotoxic and cytotoxic effect evaluation

Cytotoxicity and genotoxicity assays on human neuronal cells (HTLA) were performed on **8a** and **11b**, selected on the basis of their enzymatic profile. For the cytotoxic potential, we analysed the lactate-dehydrogenase release in cells exposed for 24 h to a single high concentration (100 μM) of test compounds and **1** (as reference compound). The results clearly indicate that none of the tested compounds exerted cytotoxic effects (Table 5).

To evaluate genotoxicity, we analysed the phosphorylation of the chromatin-bound histone H2AX (γ-H2AX), which is a quantitative marker for the DNA damage response at the site of double-strand breaks [38]. To this end, we performed immunoblot analysis on protein extracts from HTLA cells exposed for 24 h to the different compounds. As a positive control, we used etoposide, a topoisomerase II inhibitor that induces DNA double-stranded breaks [39]. As shown in Fig. 5, the etoposide treatment of HTLA cells led to a robust DNA damage, whereas compounds **8a**, **11b**, as well as **1**, did not produce the γ-H2AX immunoreactive band, typical marker of genotoxicity.

2.5. In vitro cAMP-enhancing potential

To verify the capability of enhancing the intracellular accumulation of cAMP, we used a cAMP-specific enzymatic immunoassay (EIA) in HTLA cells exposed for 30 min to compound **8a** and **11b,** which have been selected on the basis of their PDE4D3 inhibitory activity, PDE4D3 selectivity, and lack of cytotoxic and genotoxic effects. Compound **1** was used as a positive control. In order to increase the basal level of cAMP, the cells received forskolin (FSK), a specific activator of adenylyl cyclase, during the last 20 min of incubation.

All tested compounds, including the reference compound **1**, were able to significantly increase the FSK-induced cAMP accumulation, without affecting the basal levels of the cyclic nucleotide. However, compared with **1**, compounds **8a** and **11b** showed a higher efficacy in increasing the intracellular cAMP level (Fig. 6).

Table 4
Calculated ADMET descriptors related to metabolism, excretion and toxicity properties.

Comp.	P-glycoprotein		Endocrine system disruption[a]		CYP3A4		LD_{50} (mg/kg)[b] (R.I. ≥ 0.30)
	Inhibitor	Substrate (R.I. ≥ 0.30)	LogRBA>−3 (R.I. ≥ 0.60)	LogRBA >0 (R.I. ≥ 0.75)	Inhibitor	Substrate (R.I. ≥ 0.30)	
1	Not	Not	0.08	0.01	Not	0.90	1400
3b	Not	Not	0.10	0.01	Not	0.89	660
8a	Not	Possible	0.07	0.01	Not	0.85	640
8b	Not	Not	0.06	0.01	Not	0.89	700
11b	Not	Not	0.09	0.01	Not	0.89	650
4b	Not	Not	0.09	0.01	Not	0.94	740
4d	Not	Not	0.07	0.01	Not	0.88	870
4g	Not	Not	0.03	0.01	Not	0.82	1400
Rolipram	Not	Not	0.05	0.00	Not	0.53	660
Roflumilast	Not	Not	0.07	0.00	Not	0.58	1200

[a] RBA represents the relative binding affinity with respect to that of estradiol. Compounds showing LogRBA > 0 are classified as strong estrogen binders, while those showing LogRBA < −3 are considered as non-binders.
[b] Lethal dose 50% (LD_{50}) for mouse after oral administration (RI: reliability index. Borderline-allowed values for reliability parameter are ≥0.3, the most predictive fall in the range 0.50–1.0).

Table 5
Cytotoxic potential of compounds **8a**, **11b** and **1**[a].

Compounds	Cytotoxicity %
Positive control	100 ± 8.0
DMSO	3.73 ± 1.2
8a	3.30 ± 0.4
11b	0.79 ± 0.8
1	0.70 ± 0.9

[a] Data are expressed as percent of positive control (100% cytotoxicity). Cells were exposed to the different compounds (100 μM) or to an equal volume of solvent (DMSO) for 24 h and conditioned media were then analysed for lactate-dehydrogenase release. Compound **1** has been used as reference compound. Data show mean ± SD for at least three independent experiments.

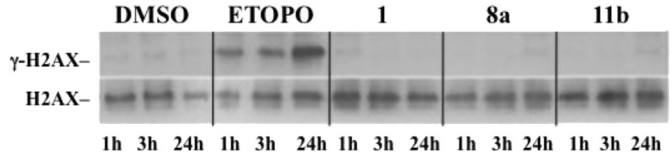

Fig. 5. Genotoxic potential of compounds **8a, 11b** and **1**. Western blot analysis of γ-H2AX in HTLA cells treated for 1, 3 and 24 h with 100 μM of **1**, **8a**, **11b**, etoposide (positive control) or with an equal volume of solvent (DMSO). The H2AX signals represent the internal loading control. Compound **1** has been used as reference compound. Each figure is representative of three independent experiments all showing essentially similar results.

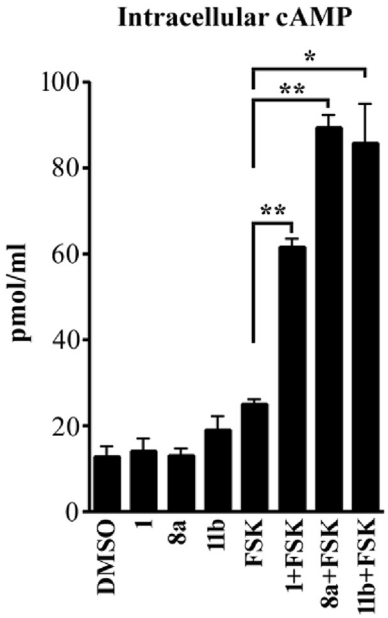

Fig. 6. In vitro cAMP-enhancing potential of compounds **8a, 11b** and **1** in cultured cells. Neuronal cultured cells were pre-treated for 10 min with tested compounds or an equal volume of DMSO. Then, 1 μM forskolin (FSK) was added, where indicated, for 20 min. At the end of the incubation periods, intracellular cAMP was measured with a cAMP-specific EIA kit, accordingly to the manufacturer's instructions. Compound **1** has been used as reference compound. Data show mean ± SEM for 3 independent experiments. *$p < 0.05$; **$p < 0.01$ vs FSK.

2.6. In vivo pharmacokinetic study

Pharmacokinetic analysis of compounds **8a** and **11b** was performed in BALB/c mice following s.c. administration of a 10 mg/kg dose. The main pharmacokinetic parameters of the two compounds are summarized in Table 6, together with those previously reported for compound **1** [31].

Data showed that compounds **8a** and **11b** were rapidly absorbed, as indicated by the respective plasma Tmax of 0.17 h and 0.5 h, and rapidly eliminated with a respective plasma half-life of 0.78 h and 0.97 h. The brain distribution of compound **8a** was also fast (brain Tmax 0.17 h) and its brain/plasma (b/p) ratio ranged from 74.6 to 81.4% (calculated using $AUC_{0\text{-}t}$ or C_{max}, respectively). The concentration of compound **11b** in mouse brain tissue peaked at 0.5 h after administration and the b/p ratio (calculated using C_{max}) was 8.4%

In conclusion, compounds **8a** and **11b** were rapidly absorbed and were able to readily reach the brain. Compound **11b**, however,

Table 6
Main pharmacokinetic parameters of compounds **8a**, **11b** and **1**[a].

Compounds	8a		11b		**1**[b]	
Parameters	Plasma	Brain	Plasma	Brain	Plasma	Brain
T_{max} (h)	0.17	0.17	0.5	0.5	0.17	0.17
C_{max} (ng/mL or g)	3650	2970	1225	103	4406	1567
$t_{1/2}$ (h)	0.78	0.58	0.97	nd[c]	0.7	1.36
$AUC_{0\text{-}t}$ (ng·h/mL or g)	1051	784	845	nd	1225	391

[a] Analyses were performed in mice following s.c. administration of a 10 mg/kg dose. Compound **1** has been used as reference compound.
[b] Results taken from Ref. [31].
[c] nd = not determined.

showed a rather poor brain penetration, whereas compound **8a** demonstrated a b/p ratio of 0.75–0.81, which is greatly improved with respect to both compound **1** (b/p ratio 0.32–0.35) and other recently reported analogues [31]. Thus, on the basis of its more favourable selectivity and pharmacokinetic profiles, we choose compound **8a** for further in vivo studies.

2.7. In vivo cAMP-enhancing potential

In these experiments, we have evaluated the in vivo effects of compound **8a** on extracellular cAMP levels in the hippocampus of freely moving rats by means of intracerebral microdialysis. Intrahippocampal administration of compound **8a,** at the concentration of 30 μM, caused a slight, though not significant, increase of extracellular cAMP (Fig. 7). However, when the PDE4D inhibitor was infused at the concentration of 100 μM, a marked cAMP response could be observed (40–80% over basal values). The effects of compound **8a** were similar to those previously reported for the PDE4D inhibitor **1** [31].

2.8. Behavioral studies

2.8.1. Effects of compound *8a* on natural forgetting of rats in the ORT

The object recognition task (ORT) is a one-trial learning task for episodic-like memory in rodents [40] and it measures if rodents recognize/remember that an object from the learning trial has been replaced with a different object. The specific timing of the treatment, in relation to the learning or test trial, allows one to investigate acquisition, consolidation or retention memory processes [41,42].

Untreated healthy rodents do not remember the familiar object after a 24 h inter-trial interval [43] and, therefore, this ORT inter-trial interval can be used to measure enhancements in episodic-like memory.

The studies in healthy 4–5 months-old male Wistar rats were designed to find the efficacious dose-range of **8a,** administered intraperitoneally at the optimum time point of 3 h after the learning trial [44], on natural forgetting in the ORT, using a 24 h inter-trial interval. The results of the dose-response experiment with this compound are summarized in Table 7. One-sample *t*-test, comparing the d2 index of every condition to zero (chance level), showed that vehicle, 0.001 and 0.01 mg/kg **8a** did not significantly differ from zero, implying no recognition of the familiar object after a 24 h interval. On the contrary, 0.003 mg/kg of **8a** showed a significant difference compared to zero ($P < 0.001$). A one-way ANOVA revealed a significant difference in the ORT performance of the treatment conditions ($F_{3,63} = 2.988$; $P = 0.0376$). Post-hoc Dunnett's *t*-test, comparing every treatment to vehicle, showed that the dose of 0.003 mg/kg could significantly enhance ORT memory performance in rats ($P < 0.05$). In summary, from the doses tested (0.001, 0.003 and 0.01 mg/kg i.p.), 0.003 mg/kg of **8a** was able to fully enhance memory performance compared to vehicle treatment. Fig. 8 gives a visual representation of these results.

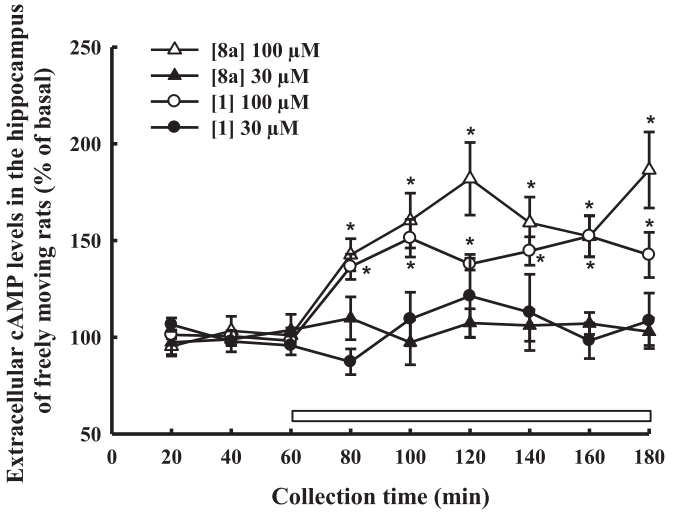

Fig. 7. In vivo cAMP-enhancing effects of compounds **8a** and **1**in rat hippocampus. Compounds **8a** or **1** were administered through the microdialysis probe after 3 consecutive control samples had been collected and were present in the infusion fluid for the time indicated by the horizontal empty bar. Data are expressed as percentages of the mean basal value (defined 100%) that was determined by averaging the cAMP content in the three fractions collected before drug treatment. Data represent mean ± SEM of 5–6 different experiments. Data for compound **1** were taken from Ref. [13]. *p < 0.05 vs mean basal values.

2.8.2. Effects of compound *8a* on a scopolamine-induced memory deficit of rats in the ORT

Compound **8a** was also tested in a scopolamine-induced model of memory impairment in the same paradigm to investigate its effect on a memory deficit. Scopolamine (0.1 mg/kg) impairs memory in the ORT at a 1 h inter-trial interval. Doses of 0.001, 0.003 and 0.01 mg/kg of **8a** were administrated prior to trial 1 to evaluate their effects on the scopolamine induced memory deficit.

The ORT measures of this study are given in Table 8. The animals that received scopolamine and vehicle did not recognize the familiar object after one hour, as measured with one-sample *t*-test comparing the d2 index with zero. The vehicle + vehicle treated rats did show a significantly higher performance compared to zero ($P < 0.001$), implying that the scopolamine model for memory impairment worked in these animals. Furthermore, the scopolamine +0.003 mg/kg **8a** treated animals also showed a significantly higher performance than chance level ($P < 0.001$).

A one-way ANOVA, comparing the d2 index of all treatment conditions, showed a significant effect ($F_{4,71} = 4.876$; $P = 0.0016$). Dunnett's post-hoc test indicated that both the vehicle + vehicle ($P < 0.01$) and the scopolamine + 0.003 mg/kg **8a** ($P < 0.001$) treated animals had a significantly higher ORT performance. These results imply that the dose of 0.003 mg/kg of **8a** is able to fully reverse the scopolamine-induced memory deficit in rats. A graphical representation of these results is depicted in Fig. 9.

2.8.3. Effects of compound *8a* on emetic-like behavior of rats in the xylazine/ketamine anaesthesia test

The xylazine/ketamine-induced α_2-adrenoceptor-mediated anaesthesia test [45] was used to investigate the potential emetic properties of compound **8a,** administered at doses up to one hundred times higher than that effective in the ORT (0.003, 0.03 and 0.3 mg/kg). The results of this test are summarized in Table 9. An

Table 7
Mean values of the different ORT measures on natural forgetting with compound **8a**.[a]

Dose	e1 (s)	e2 (s)	d2	N
Vehicle	26.94 (3.07)	33.24 (2.48)	0.05 (0.05)	22
0.001 mg/kg	28.65 (2.95)	37.21 (3.49)	0.08 (0.09)	15
0.003 mg/kg	31.78 (4.10)	41.41 (2.94)	0.31 (0.06)###	15
0.01 mg/kg	24.22 (2.81)	33.79 (3.21)	0.09 (0.08)	15

[a] Data report the mean exploration time in T1 (e1) and T2 (e2) and discrimination performance (d2) of the different treatment conditions in the **8a** dose-response study. The Standard Error of the Mean (SEM) is presented between brackets. One sample *t*-tests were performed on the d2 measures. A significant difference from zero (###p < 0.001) indicates that the rats remembered the object from T1.

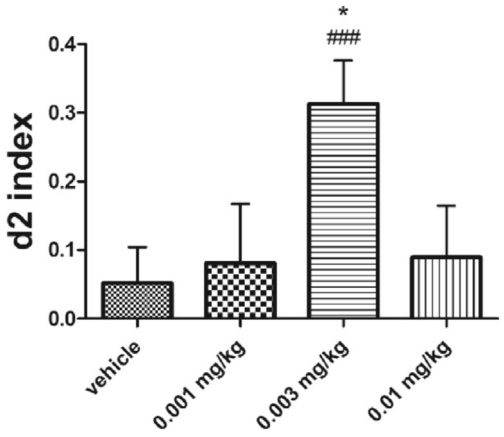

Fig. 8. The effect of compound **8a** on ORT memory performance in healthy rats using a 24 h interval. Figure shows the average d2 value and SEM of each treatment condition in the **8a** dose-response study. The discrimination index (d2) is indicated on the y-axis and the different treatment conditions are shown on the x-axis. $^{###}p < 0.001$ vs zero; $^{*}p < 0.05$ vs vehicle.

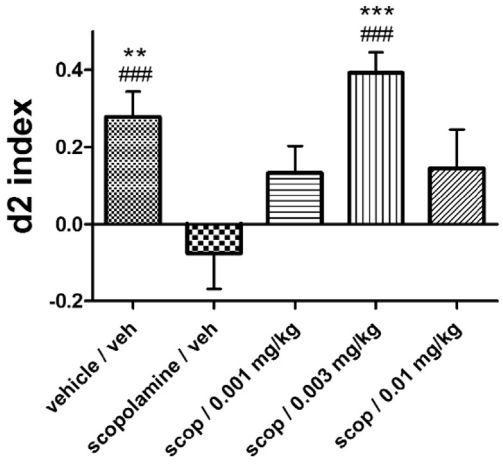

Fig. 9. The effect of compound **8a** on ORT performance in rats with a scopolamine-induced memory deficit. Figure shows the average d2 value (±SEM) of each treatment condition in the scopolamine-induced memory deficit study. The discrimination index (d2) is indicated on the y-axis and the different treatment conditions are shown on the x-axis. $^{###}p < 0.001$ vs zero; $^{**}p < 0.01$ and $^{***}p < 0.001$ vs scopolamine/vehicle.

Table 8
Mean values (±SEM) of the different ORT measures on a memory deficit model with compound **8a**[a].

Dose	e1 (s)	e2 (s)	d2	n
Vehicle + vehicle	38.37 (5.58)	27.64 (3.44)	0.28 (0.07)###	17
Scopolamine + vehicle	22.65 (4.88)	23.33 (4.23)	−0.08 (0.09)	15
Scop + 0.001 mg/kg	25.80 (4.50)	29.60 (3.22)	0.13 (0.07)	15
Scop + 0.003 mg/kg	24.36 (5.60)	21.07 (2.10)	0.39 (0.05)###	14
Scop + 0.01 mg/kg	22.65 (2.48)	25.20 (2.17)	0.14 (0.10)	15

[a] Data report the mean exploration time in T1 (e1) and T2 (e2) and discrimination performance (d2) of the different treatment conditions in the **8a** dose-response study. The Standard Error of the Mean (SEM) is presented between brackets. One sample *t*-tests were performed on the d2 measures. A significant difference from zero ($^{###}p < 0.001$) indicates that the animals remembered the object from T1.

Table 9
Mean anaesthesia times in the xylazine/ketamine test on compound **8a**[a].

Condition	Time anaesthetized	SEM	n
Vehicle	100.0	6.85	15
0.003 mg/kg	112.76	8.67	12
0.03 mg/kg	104.14	7.42	10
0.3 mg/kg	94.26	4.22	15

[a] Data are reported as percentage variations (±SEM) induced by compound **8a** relative to vehicle (set at 100%).

anaesthesia time shorter than that of the vehicle condition would implicate emetic-like effects [45]. Anaesthesia time was calculated relatively to the vehicle condition, which was set at 100%. A one-way ANOVA, comparing all conditions, did not show any significant effect ($F_{3,48} = 1.643$; n.s.), implying that **8a** does not have emetic-like effects in healthy adult rats.

3. Conclusions

Starting from our previous computational and pharmacological studies on several series of our PDE4D inhibitors, we designed a new library of catechol-based derivatives where the iminoether function has been replaced by five membered heterocycles (isoxazole, isoxazolines, and pyrazole) bearing conserved alkyl chains.

The preliminary enzymatic screening performed on human PDE4D3 isoform, evidenced a different behavior for each structural subfamily. In particular, the inclusion of the C═N–O–C– moiety, typical of previous compounds, in a more planar and rigid ring (e.g. isoxazole derivatives **5**–**7)** was detrimental for the inhibitory activity. Among the most flexible isoxazolines (compounds **3** and **4**), only **4b**, **4d** and **4g** showed satisfactory PDE4D3 inhibition, with **4b** being more selective toward the PDE4D3 isoform. The isoster pyrazole series **8a**–**c** and **11a**,**b** showed the most interesting enzymatic profile. The molecular dynamics simulation studies, performed on the isoxazoline derivative **4b** and on the pyrazole **8a**, highlighted the pivotal role of the iminoether function (but also of the alkyl chain) in establishing a stable interaction with the enzyme. In particular, the strong polarity of alkyl chain is responsible for **8a** selectivity toward PDE4D in respect to the more lipophilic PDE4B, as we have already observed in other analogue compounds [30]. Moreover, MD simulation also evidenced a different binding mode of **8a** in respect to our lead **1** [32]. Moreover, **8a** is anchored to the metal pocket in a similar manner to roflumilast suggesting that it may be considered a “typical” PDE4D inhibitor. However, we can not exclude a possible interaction of the terminal chain amino residue outside the catalytic domain; in that case our compounds may be also classified as “atypical”. New studies aiming at elucidating the co-crystallized structure of **8a** with PDE4D3 enzyme are ongoing in order to definitively dispel any doubts in this regard.

Our in silico study evidenced good ADMET properties, then confirmed by experimental data showing that the most active compounds **11b** and **8a** lacked cytotoxic and genotoxic effects.

From a functional point of view, **11b** and **8a** were able to significantly increase cAMP level in cultured cells, and compound **8a** also increased cAMP levels in the hippocampus in vivo, similarly to our lead **1** [13]

In the pharmacokinetic analysis, compounds **8a** and **11b** were rapidly absorbed and were able to readily reach the brain. However, **11b** showed a rather poor brain penetration in comparison with **8a** that was, therefore, selected for testing in the behavioral studies. Of note, the brain/plasma ratios for roflumilast and rolipram are approximately 1 and 2, respectively [46]. Thus, our compound **8a**, having a brain/plasma ratio of 0.8, is almost equal or half as brain penetrant as roflumilast and rolipram, respectively.

In a natural forgetting paradigm, **8a** was able to significantly enhance long-term memory performance of rats in the ORT at the dose of 0.003 mg/kg. The same dose was able also to fully reverse the scopolamine induced short-term memory deficit in rats, up to the level of the memory performance of control animals. For

comparison, the effective dose of **8a** in these behavioral paradigms is 10 times lower than that of roflumilast and rolipram [13,46,47]. Finally, the most interesting finding is that **8a** did not have emetic-like effects in the xylazine/ketamine anaesthesia test at doses 100 times higher than that improving memory.

In previous studies, roflumilast showed emetic-like effects at a dose 100 times higher than that improving ORT performance in rodents, while for rolipram this side effect was observed at the same or at a10 times higher dose [46,13].

Based on our results, it is evident that, compared to rolipram, our compound **8a** is more selective for PDE4D3 than for the other PDE4 isoforms, i.e. PDE4A4, PDE4B2 and PDE4C2. However, when comparing IC_{50} values, **8a** is less potent than rolipram on PDE4D. Indeed, the IC_{50} values of all the synthesized compounds are in the micromolar range, suggesting that they reflect binding to the low affinity binding site of the enzyme (i.e. the catalytic domain). Interestingly, **8a** is 10 times more effective in improving memory performance than roflumilast and rolipram, while it is less brain penetrant and has a much higher IC_{50} value for the PDE4D3 isoform than roflumilast and rolipram [46]. In addition, its emetic-like potential is greatly reduced compared to roflumilast and rolipram [46]. Thus, **8a** displays a dissociation between its memory improving effect and reduced emetic-like potential. One possible explanation could be that the IC_{50} values of the catalytic site/full enzyme are not strictly related to behavior. Linked to this, it might be possible that 8a causes inhibition of specific PDE4D isoforms involved in memory processes and not those in emesis. Lastly, since PDE4B is also emetic and **8a** is less selective for this isoform, this might also contribute to a reduced emetic potential of this compound [48]. All these assumptions clearly need attention in future research.

In conclusion, compound **8a** is a selective PDE4D inhibitor that is able to enhance memory performance without toxic and emetic effects, thus representing a promising candidate for further lead optimization and preclinical evaluations.

4. Experimental

4.1. Chemistry

All chemicals were purchased from Chiminord and Aldrich Chemical, Milan, Italy. Solvents were reagent grade. Unless otherwise stated, all commercial reagents were used without further purification.

Aluminium backed silica gel plates (Merck DC-Alufolien Kieselgel 60 F254, Darmstad, Germany), were used in thin-layer chromatography (TLC) for routine monitoring the course of reactions. Detection of spots was made by UV light. Merck silica gel, 230–400 mesh, was used for chromatography.

All the amines were purified by distillation before the use. Melting points are not "corrected" and were measured with a Buchi M-560 instrument. IR spectra were recorded with a Perkin-Elmer 398 spectrophotometer. ^{1}H NMR spectra were recorded on a Varian Gemini 200 (200 MHz) or a Bruker DPX300 (300 MHz) instruments and chemical shifts are reported as δ (ppm) relative to tetramethylsilane (TMS) as internal standard; signals were characterized as s (singlet), d (doublet), t (triplet), m (multiplet), br s (broad signal); J in Hz. MS spectra were recorded on HP 6890-5973 apparatus: injection temperature 250 °C, HP5 poly(-methylphenylsilxane) column 30 m x 0,25 mm, He flux 1 mL/min.

Elemental analyses were determined with an elemental analyzer EA 1110 (Fison-Instruments, Milan, Italy). Analyses indicated by the symbols of the elements or functions were within ±0.4% of the theoretical values.

4.1.1. Synthesis of 3-(cyclopentyloxy)-N-hydroxy-4-methoxybenzenecarboximidoyl chloride ***14***

N-chlorosuccinimide (1.02 g, 7.67 mmol) was added to a solution of 3-(cyclopentyloxy)-4-methoxybenzaldehyde oxime **13** (1.72 g, 7.31 mmol) in an. DMF (10 mL), and the mixture was stirred at 40–45 °C for 1 h. After cooling to room temperature, water (65 mL) was added and the solution was put for 12 h in a refrigerator; afterward, water was removed and the oil residue was solved in AcOEt (20 mL), the organic phase was washed with water (3 × 20 mL), dried ($MgSO_4$) and concentrated under reduced pressure yielding a light brown oil. Yield: 65%; ^{1}H NMR ($CDCl_3$): δ 1.47–2.13 (m, 8H, 4CH_2 cyclopent.), 3.87 (s, 3H, OCH_3), 4.71–4.89 (m, 1H, OCH cyclopent.), 6.84 (d, J = 8.4 Hz, 1H, H-5 Ar), 7.35 (dd, J = 8.4, 2.0 Hz, 1H, H-6 Ar), 7.38 (d, J = 2.0 Hz, 1H, H-2 Ar); IR (film): cm^{-1} 3000–3500 (OH); Anal. ($C_{13}H_{16}ClNO_3$) calcd for C, H, N.

4.1.2. Synthesis of ethyl 3-[3-(cyclopentyloxy)-4-methoxyphenyl]-4,5-dihydroisoxazole-5-carboxylate ***15***

Ethyl acrylate (2.31 mL, 21.14 mmol) and triethylamine (TEA) (3.54 mL, 25.37 mmol) were added, under nitrogen atmosphere, to a solution of 3-(cyclopentyloxy)-*N*-hydroxy-4-methoxybenzenecarboximidoyl chloride **14** (2.85 g, 10.57 mmol) in dichloroethane (DCE) (16 mL) cooled at 0 °C.

The yellow solution was stirred at 60 °C for 1 h and at room temperature for further 48 h. Water (20 mL) was added and the mixture was extracted with dichloromethane (DCM) (3 × 10 mL). The organic phases were washed with brine (3 × 10 mL), dried ($MgSO_4$) and concentrated under reduced pressure, yielding an oil which was purified by silica gel (100–200 mesh) column chromatography using a mixture of diethyl ether/petroleum ether (boiling point 40–60 °C) (1:1) as the eluent. The final product crystallized as a light yellow solid, which was re-crystallized by diethyl ether. Yield: 50%; mp: 60 °C; ^{1}H NMR ($CDCl_3$): δ 1.36 (t, 3H, OCH_2CH_3), 1.50–2.10 (m, 8H, 4 CH_2 cyclopent.), 3.60–3.65 (m, 2H, CH_2 isoxaz.), 3.89 (s, 3H, OCH_3), 4.28 (q, 2H, OCH_2CH_3), 4.78–4.90 (m, 1H, OCH cyclopent.), 5.16 (t, J = 8.6 Hz 1H, H-5 isoxaz.), 6.86 (d, J = 8.0 Hz, 1H, H-5 Ar), 7.05 (dd, J = 8.2, 2.0 Hz, 1H, H-6 Ar), 7.37 (d, J = 2.0 Hz, 1H, H-2 Ar); Anal. ($C_{18}H_{23}NO_5$) calcd for C, H, N.

4.1.3. General procedure for the synthesis of 4-({3-[3-(cyclopentyloxy)-4-methoxyphenyl]-4,5-dihydroisoxazol-5-yl} carbonyl)amines ***3a-f***

A mixture of ethyl 3-[3-(cyclopentyloxy)-4-methoxyphenyl]-4,5-dihydroisoxazole-5-carboxylate **15** and the suitable amine was heated at 60 °C overnight. If the amine was a solid, the reaction was carried on using anhydrous dimethylformamide (DMF) (10 mL) as the solvent. After cooling to room temperature, the reaction mixture was poured into water (20 mL), yielding a crude solid that was filtered and re-crystallized from diethyl ether. If no precipitate was formed, the water suspension was extracted with DCM (3 × 10 mL), washed with 1 N HCl solution (10 mL) and brine (2 × 10 mL), dried ($MgSO_4$) and evaporated under reduced pressure. The solid obtained was re-crystallized from diethyl ether.

*4.1.3.1. 4-({3-[3-(Cyclopentyloxy)-4-methoxyphenyl]-4,5-dihydroisoxazol-5-yl}carbonyl)morpholine (**3a**).* White solid; Yield: 76%; mp: 115–116 °C; ^{1}H NMR ($CDCl_3$): δ 1.55–2.10 (m, 8H, 4CH_2 cyclopent.), 3.30–4.30 (m, 13H, CH_2 isoxazol. + 4CH_2 morph. + OCH_3), 4.78–4.90 (m, 1H, OCH cyclopent.), 5.30–5.40 (m, 1H, H-5 isoxaz.), 6.88 (d, J = 8.0 Hz, 1H, H-5 Ar), 7.13 (dd, J = 6.6, 2.0 Hz, 1H, H-6 Ar), 7.37 (d, J = 2.0 Hz, 1H, H-2 Ar); IR ($CHCl_3$): cm^{-1} 1650 (CO); Anal. ($C_{20}H_{26}N_2O_5$) calcd for C, H, N.

4.1.4. Synthesis of {3-[3-(cyclopentyloxy)-4-methoxyphenyl]-4,5-dihydroisoxazol-5-yl}acetic acid **16**

3-butenoic acid (5 mL, 58.58 mmol) and TEA (9.8 mL, 70 mmol) were added, under nitrogen atmosphere, to a solution of 3-(cyclopentyloxy)-*N*-hydroxy-4-methoxybenzenecarboximidoyl chloride **14** (7.9 g, 29.29 mmol) in DCE (46 mL) cooled at 0 °C and the solution was stirred at 60 °C for 1.5 h and at room temperature for further 48 h. Water was added (20 mL) and the mixture was extracted with DCM (3 × 10 mL). The organic phases were washed with a $NaHCO_3$ saturated solution (2 × 10 mL); then, the aqueous phase was treated with 1 N HCl until precipitation of the final product as a white solid. Yield: 35%; mp: 126–128 °C; ^{1}H NMR ($CDCl_3$): δ 1.50–2.10 (m, 8H, $4CH_2$ cyclopent.), 2.65–3.05 (m, 2H, CH_2COOH), 3.05–3.65 (m, 2H, CH_2 isoxaz.), 3.90 (s, 3H, OCH_3), 4.78–4.95 (m, 1H, OCH cyclopent.), 5.05–5.20 (m, 1H, H-5 isoxaz.), 6.86 (d, J = 8.0 Hz, 1H, H-5 Ar), 7.06 (dd, J = 8.2, 2.0 Hz, 1H, H-6 Ar), 7.38 (d, J = 2.0 Hz, 1H, H-2 Ar), 8.05 (br s, 1H, COOH, disappears with D_2O); Anal. ($C_{17}H_{21}NO_5$) calcd for C, H, N.

4.1.5. General procedure for the synthesis of 4-({3-[3-(cyclopentyloxy)-4-methoxyphenyl]-4,5-dihydroisoxazol-5-yl} acetyl)amines **4a–g** (method A)

TEA (0.31 mL, 2.25 mmol), the suitable amine (3 mmol) and diphenylphosphorylazide (DPPA) (0.36 mL, 1.65 mmol) were added to a solution of {3-[3-(cyclopentyloxy)-4-methoxyphenyl]-4,5-dihydroisoxazol-5-yl}acetic acid **16** (0.48 g, 1.5 mmol) in anhydrous DMF (4 mL), cooled in an ice-water bath, and the reaction mixture was heated at 80 °C for 24 h. After cooling to room temperature, the reaction mixture was poured into water (50 mL), extracted with DCM (3 × 10 mL), washed with a $NaHCO_3$ saturated solution (10 mL), 1 N HCl solution (10 mL) and brine (2 × 10 mL), dried ($MgSO_4$) and evaporated under reduced pressure. The solid obtained was purified by crystallization from diethyl ether.

4.1.5.1. 4-({3-[3-(Cyclopentiloxy)-4-methoxyphenyl]-4,5-dihydroisoxazol-5-yl}acetyl)(2,6-dimethyl)morpholine **4b**.

White solid. Yield: 38%; mp: 104–105 °C. ^{1}H NMR ($CDCl_3$): δ 1.00–1.43 (m, 6H, $2CH_3$ morph.), 1.48–2.13 (m, 8H, $4CH_2$ cyclopent.), 2.20–4.20 (m, 10H, 2CHO morph. + $2CH_2N$ morph. + CH_2 isoxaz. + CH_2CO), 3.90 (s, 3H, OCH_3), 4.65–4.96 (m, 1H, OCH cyclopent.), 5.05–5.28 (m, 1H, H-5 isoxaz.), 6.87 (d, J = 8.0 Hz, 1H, H-5 Ar), 7.08 (dd, J = 8.0, 2.0 Hz, 1H, H-6 Ar), 7.37 (d, J = 1.6 Hz, 1H, H-2 Ar). Anal. ($C_{23}H_{32}N_2O_5$) calcd for C, H, N.

4.1.6. General procedure for the synthesis of 4-({3-[3-(cyclopentyloxy)-4-methoxyphenyl]-4,5-dihydroisoxazol-5-yl} acetyl)amines **4a,b** (method B)

The suitable 1-amino-3-buten-1-one **17a** or **17b** (22 mmol) solved in anydrous DMF (10 mL) was added dropwise, at 0 °C and under nitrogen atmosphere, to a solution of 3-(cyclopentyloxy)-*N*-hydroxy-4-methoxybenzenecarboximidoyl chloride **14** (2.97 g, 11 mmol) in anydrous DMF (20 mL); then, TEA (1.72 g, 17 mmol, 2.37 mL). The mixture was stirred at room temperature for 72 h, cooled to room temperature and poured into water (100 mL). The mixture was extracted with diethyl ether (3 × 20 mL), the organic phase was washed with brine (3 × 20 mL), dried ($MgSO_4$) and concentrated under reduced pressure. Compound **4a** was obtained as a yellow solid that was re-crystallized by anhydrous methanol. Compound **4b** was purified by silicagel (100–200 mesh) column chromatography using diethyl ether as the eluent to afford a pure product as a white solid.

4.1.6.1. 4-({3-[3-(Cyclopentyloxy)-4-methoxyphenyl]-4,5-dihydroisoxazol-5-yl}acetyl)morpholine (**4a**).

Yield: 41%; mp: 144 °C.

4.1.6.2. 4-({3-[3-(Cyclopentiloxy)-4-methoxyphenyl]-4,5-dihydroisoxazol-5-yl}acetyl)(2,6-dimethyl)morpholine (**4b**).

Yield: 40%; mp: 104–105 °C.

4.1.7. General procedure for the synthesis of 1-(4-morpholinyl)-3-buten-1-one and 1-(2,6-dimethyl-4-morpholinyl)-3-buten-1-one **17a,b**

Thionyl chloride (9.68 g, 81.31 mmol, 5.9 mL) was added dropwise to 3-butenoic acid (5 g, 58.08 mmol, 4.9 mL) cooled at 0 °C. The mixture was refluxed for 30 min, then cooled at 0 °C. The suitable cycloamine (114 mmol), solved in anydrous THF (25 mL), was added and the mixture was stirred at room temperature for 2 h. The solid was filtered off, washed with an. THF and the collected organic phases were evaporated under reduced pressure. A $NaHCO_3$ saturated solution (100 mL) was added to the crude and the mixture was extracted with DCM (3 × 20 mL), the organic phase was washed with water (20 mL), dried ($MgSO_4$) and concentrated under reduced pressure. The crude was purified by high vacuum distillation (95 °C/1 mmHg) to afford the pure products as a light yellow oil.

4.1.7.1. 1-(4-Morpholinyl)-3-buten-1-one (**17a**).

Yield: 67%; ^{1}H NMR ($CDCl_3$): δ 3.00–3.13 (m, 2H, CH_2CO), 3.30–3.65 (m, 8H, $4CH_2$ morph.), 4.95–5.15 (m, 2H, CH_2=CH), 5.75–5.93 (m, 1H, CH_2=CH): IR ($CHCl_3$) cm^{-1}: 1633 (CO); GC-MS *m/z*: 155 (M^+), 56, 70, 86, 114.

4.1.8. Synthesis of 1-{3-[3-(cyclopentyloxy)-4-methoxyphenyl] isoxazol-5-yl}ethanol 18

3-butyn-2-ol (0.36 mL, 4.56 mmol) and, subsequently, TEA (0.95 mL, 6.84 mmol) were added dropwise to a solution of 3-(cyclopentyloxy)-*N*-hydroxy-4-methoxybenzenecarboximidoyl chloride **14** (1.23 g, 4.56 mmol) in an. toluene (5 mL) cooled at 0–5 °C; then, the mixture was heated at 60 °C for 18 h. After cooling to room temperature, the mixture was filtered and the solid obtained was washed with an. toluene (3 × 10 mL). The collected organic phases were washed with water (3 × 20 mL), dried ($MgSO_4$) and concentrated under reduced pressure yielding a yellow oil which was purified by Florisil (100–200 mesh) column chromatography using diethyl ether as the eluent. The crude crystallized as a white solid by addition of a mixture of diethyl ether/petroleum ether (bp 40–60 °C) (1:1). Yield: 60%; mp: 72–73 °C; ^{1}H NMR ($CDCl_3$): δ 1.62 (d, J = 6.6 Hz, 3H, CH_3), 1.75–2.10 (m, 8H, $4CH_2$ cyclopent.), 2.02 (s, 1H, OH, disappears with D_2O), 3.87 (s, 3H, OCH_3), 4.75–4.91 (m, 1H, OCH cyclopent.), 4.95–5.11 (m, 1H, CHOH), 6.44 (s, 1H, H-5 isoxaz.), 6.88 (d, J = 8.2 Hz, 1H, H-5 Ar), 7.24 (dd, J = 8.2, 2.0 Hz, 1H, H-6 Ar), 7.37 (d, J = 2.0 Hz, H-2 Ar); IR (KBr) cm^{-1}: 3398 (OH); Anal. ($C_{17}H_{21}NO_4$) calcd for C, H, N.

4.1.9. Synthesis of 1-{3-[3-(cyclopentyloxy)-4-methoxyphenyl] isoxazol-5-yl}ethanone **19**

Acetic anhydride (13.78 mL) was added to 1-{3-[3-(cyclopentyloxy)-4-methoxyphenyl]isoxazol-5-yl}ethanol**18** (4.18 g, 13.78 mmol) in DMSO (21 mL), and the solution was stirred at room temperature for 24 h. Then, water (230 mL) was added and the solid obtained was filtered and re-crystallized by absolute ethanol yielding a white solid. Yield: 80%; mp: 121–122 °C; ^{1}H NMR ($CDCl_3$): δ 1.42–2.10 (m, 8H, $4CH_2$ cyclopent.), 2.63 (s, 3H, CH_3), 3.88 (s, 3H, OCH_3), 4.75–4.94 (m, 1H, OCH cyclopent.), 6.91 (d, J = 8.2 Hz, 1H, H-5 Ar), 7.13 (s, 1H, H-5 isoxaz.), 7.26 (dd, J = 8.2, 2.0 Hz 1H, H-6 Ar), 7.39 (d, J = 2.0 Hz, H-2 Ar); IR (KBr) cm^{-1}: 1696 (CO); Anal. ($C_{17}H_{19}NO_4$) calcd for C, H, N.

4.1.10. Synthesis of 2-bromo-1-{3-[3-(cyclopentyloxy)-4-methoxyphenyl]isoxazol-5-yl}ethanone **20**

Glacial acetic acid (0.05 mL) was added to a solution of 1-{3-[3-

(cyclopentyloxy)-4-methoxyphenyl]isoxazol-5-yl}ethanone **19** (0.56 g, 1.86 mmol) in DCM (3 mL), and the reaction mixture was heated at 50 °C. Afterward, a solution of bromine (0.1 mL, 1.95 mmol) in DCM (1 mL) was added dropwise and the mixture was heated at reflux for 1 h. After cooling to room temperature, the suspension was diluted with DCM (20 mL), washed once with ice-water (20 mL), then with water (2 × 20 mL), dried ($MgSO_4$) and concentrated under reduced pressure yielding a yellow solid which was re-crystallized by absolute ethanol to give the final product as a white solid. Yield: 60%; mp: 120–122 °C; ^{1}H NMR ($CDCl_3$): δ 1.57–2.14 (m, 8H, $4CH_2$ cyclopent.), 3.89 (s, 3H, OCH_3), 4.47 (s, 2H, CH_2Br), 4.78–4.93 (m, 1H, OCH cyclopent.), 6.93 (d, J = 8.2 Hz, 1H, H-5 Ar), 7.20–7.37 (m, 2H, H-6 Ar + H-5 isoxaz.), 7.41 (d, J = 1.8 Hz, H-2 Ar); IR (KBr) cm^{-1}: 1698 (CO); Anal. ($C_{17}H_{18}BrNO_4$) calcd for C, H, N.

4.1.11. General procedure for the synthesis of 1-{3-[3-(cyclopentyloxy)-4-methoxyphenyl]isoxazol-5-yl}-2-cycloaminoethanones **5a,b**

The suitable cycloamine (2.91 mmol) was added to a solution of 2-bromo-1-{3-[3-(cyclopentyloxy)-4-methoxyphenyl]isoxazol-5-yl}ethanone **20** (0.54 g, 1.42 mmol) in DCM (3 mL), cooled at −10 °C (for compound **5a**) or at −30 °C (for compound **5b**). After a few minutes, the reaction was completed and a saturated solution of anhydrous HCl in diethyl ether was immediately added to the reaction mixture, yielding the hydrochloride salts of compounds **5a,b** as white solids.

4.1.11.1. 1-{3-[3-(Cyclopentyloxy)-4-methoxyphenyl]isoxazol-5-yl}-2-morpholin-4-ylethanone hydrochloride (**5a**).

Yield: 72%; mp: 175 °C (dec.); ^{1}H NMR ($CDCl_3$): δ 1.60–2.20 (m, 8H, $4CH_2$ cyclopent.), 3.60–3.80 (m, 4H, $2CH_2N$ morph.), 4.07 (s, 3H, OCH_3), 4.20–4.50 (m, 4H, $2CH_2O$ morph.), 4.27 (s, 2H, CH_2N), 4.95–5.10 (m, 1H, OCH cyclopent.), 7.08 (d, J = 2.0 Hz, 1H, H-5 Ar), 7.35–7.52 (m, 3H, H-2 Ar + H-5 isoxaz. + NH^+, 1H disappears with D_2O), 7.55 (d, J = 2.0 Hz, 1H, H-6 Ar); IR (KBr) cm^{-1}: 1710 (CO); Anal. ($C_{21}H_{26}N_2O_5$.HCl) calcd for C, H, N.

4.1.12. General procedure for the synthesis of 1-{3-[3-(cyclopentyloxy)-4-methoxyphenyl]isoxazol-5-yl}-2-cycloaminoethanols **6a-b**

$NaBH_4$ (0.041 g, 1.1 mmol) was added portion-wise, at room temperature, to a suspension of 1-{3-[3-(cyclopentyloxy)-4-methoxyphenyl]isoxazol-5-yl}-2-cycloaminoethanones hydrochloride **5a** or **5b** (1.1 mmol) solved in anydrous methanol, $NaBH_4$ (0.041 g, 1.1 mmol). Afterward, a solution of sodium methoxide (60 mg, 1.1 mmol) in anydrous methanol (10 mL) was added dropwise and the mixture was stirred at room temperature for 4 h. Then, the solvent was removed under reduced pressure and the crude was solved in DCM (20 mL), washed with water (3 × 20 mL), dried ($MgSO_4$) and concentrated under reduced pressure. The morpholino derivative **6a** was obtained as a yellow solid, which was washed with hot diethyl ether. The dimethylmorpholino derivative **6b** was obtained as oil, which was purified by Florisil (100–200 mesh) column chromatography using diethyl ether as eluent. The solids obtained were further purified by preparative TLC (Silicagel) using diethyl ether as eluent, yielding the final pure products as white solids.

4.1.12.1. 1-{3-[3-(Cyclopentyloxy)-4-methoxyphenyl]isoxazol-5-yl}-2-morpholin-4-ylethanol (**6a**).

Yield 65%; mp: 136–137 °C; ^{1}H NMR ($CDCl_3$): δ 1.70–2.30 (m, 8H, $4CH_2$ cyclopent.), 2.55–2.75 (m, 2H, CH_2N), 2.80–3.00 (m, 4H, $2CH_2N$ morph.), 3.85–4.10 (m, 5H, $2CH_2O$ morph. + OH, 1H disappears with D_2O), 4.05 (s, 3H, OCH_3), 4.85–5.15 (m, 2H, OCH cyclopent. + *CH*OH), 6.71 (s, 1H, H-5 isoxaz.), 7.08 (d, J = 2.0 Hz, 1H, H-5 Ar), 7.24 (d, J = 2.0 Hz, 1H, H-6 Ar), 7.35 (s, 1H, H-2 Ar); IR (KBr) cm^{-1}: 3125 (OH); Anal. ($C_{21}H_{28}N_2O_5$) calcd for C, H, N.

4.1.13. Synthesis of methyl 3-[3-(cyclopentyloxy)-4-methoxyphenyl]isoxazole-5-carboxylate **21**

A solution of TEA (0.87 g, 8.64 mmol, 1.16 mL) in anhydrous toluene (15 mL) was added dropwise to a suspension of 3-(cyclopentyloxy)-*N*-hydroxy-4-methoxybenzenecarboximidoyl chloride **14** (2.33 g, 8.64 mmol) and methyl propiolate (0.73 g, 8.64 mmol, 0.71 mL) in anhydrous toluene (10 mL), (30 min) and the mixture was stirred at 60 °C for 12 h. After cooling to room temperature, the solid residue was filtered off and washed with anhydrous toluene. Then, the collected organic phases were dried ($MgSO_4$) and concentrated under reduced pressure, yielding a light brown oil that crystallized after addition of a mixture of diethyl ether/petroleum ether (bp 40–60 °C) (1:1) and standing overnight in a refrigerator. Yield: 33%; mp: 126–127 °C; ^{1}H NMR ($CDCl_3$): δ 1.55–2.15 (m, 8H, $4CH_2$ cyclopent.), 3.93 (s, 3H, OCH_3 Ar), 4.02 (s, 3H, OCH_3 ester), 4.82–4.96 (m, 1H, OCH cyclopent.), 6.96 (d, J = 8.2 Hz, 1H, H-5 Ar), 7.23 (s, 1H, H-5 isoxaz.), 7.30 (dd, J = 8.2, 2.2 Hz, 1H, H-6 Ar), 7.45 (d, J = 2.2 Hz, 1H, H-2 Ar); IR (KBr) cm^{-1}: 1744 (CO); Anal. ($C_{17}H_{19}NO_5$) calcd for C, H, N.

4.1.14. General procedure for the synthesis of 4-({3-[3-(cyclopentyloxy)-4-methoxyphenyl]isoxazol-5-yl}carbonyl) cycloamines **7a,b**

A suspension of methyl 3-[3-(cyclopentyloxy)-4-methoxyphenyl]isoxazole-5-carboxylate **21** (0.96 g, 2.90 mmol) and of an excess of the appropriate cycloamine (41.6 mmol) was stirred for 12 h at 60 °C. After cooling to room temperature, water (30 mL) was added and the product crystallized standing overnight in a refrigerator. The white solid obtained was filtered and re-crystallized by ethanol.

4.1.14.1. 4-({3-[3-(Cyclopentyloxy)-4-methoxyphenyl]isoxazol-5-yl}carbonyl)morpholine (**7a**).

Yield: 53%; mp: 100–101 °C; ^{1}H NMR ($CDCl_3$): δ 1.55–2.21 (m, 8H, $4CH_2$ cyclopent.), 3.92 (s, 3H, OCH_3), 3.65–3.97 (m, 8H, $4CH_2$ morph.), 4.80–4.92 (m, 1CH, OCH cyclopent.), 6.96 (d, J = 8 Hz, 1H, H-5 Ar), 7.09 (s, 1H, H isoxaz.), 7.03–7.38 (dd, J = 8.0, 1.8 Hz, 1H, H-6 Ar), 7.42 (d, J = 1.8 Hz, 1H, H-2 Ar); IR (KBr) cm^{-1}: 1636 (CO); Anal. ($C_{20}H_{24}N_2O_5$) calcd for C, H, N.

4.1.15. Synthesis of 3-[3-(cyclopentyloxy)-4-methoxyphenyl]-1H-pyrazole **22**

3-(cyclopentyloxy)-4-methoxybenzaldehyde **12** (3.90 g, 17.74 mmol), solved in anhydrous acetonitrile (10 mL), was added to a solution of *p*-toluenesulfonyl hydrazide (3.3 g, 17.74 mmol) in anydrous acetonitrile (20 mL) and the mixture was stirred at room temperature for 1 h. Then, 5 N NaOH solution (3.55 mL, 17.75 mmol) was added and the mixture, which became coloured in red, was stirred at room temperature for 20 min. Afterward, 1-vinylimidazole (8.34 g, 8.03 mL, 88.77 mmol) was slowly added and the mixture was heated at 50 °C for 48 h. After cooling to room temperature, the solvent was removed under reduced pressure and the crude was solved in ethylacetate (20 mL). The organic phase was washed with brine (2 × 20 mL), 1 N HCl solution (20 mL), water (3 × 20 mL), dried ($MgSO_4$), and concentrated under reduced pressure to obtain a light yellow oil that crystallized by addition of methanol. The pure product is obtained as a light yellow solid. Yield: 65%; mp: 80–82 °C; ^{1}H NMR ($CDCl_3$): δ 1.49–2.19 (m, 8H, $4CH_2$ cyclopent.), 3.87 (s, 3H, OCH_3), 4.72–4.97 (m, 1H, OCH cyclopent.), 6.53 (d, J = 2.2 Hz, 1H, H-4 pyraz.), 6.84–7.38 (m, 3H, 3H Ar), 7.59 (d, J = 2.2 Hz, 1H, H-5 pyraz.); IR (KBr) cm^{-1}: 3562 (NH); Anal. ($C_{15}H_{18}N_2O_2$) calcd for C, H, N.

4.1.16. Synthesis of 3-[3-(cyclopentyloxy)-4-methoxyphenyl]-1-(oxiran-2-ylmethyl)-1H-pyrazole ***23***

A mixture of 3-[3-(cyclopentyloxy)-4-methoxyphenyl]-1*H*-pyrazole **22** (0.77 g, 2.98 mmol) and epichlorohydrin (3 mL, 38.26 mmol) was cooled at 5 °C. Then, TEA (4.47 mmol, 0.62 mL) was added dropwise and the reaction mixture was stirred until the temperature became 25° and, then, heated at 70 °C for 3 h. After cooling to room temperature, the mixture was poured into water (100 mL), the aqueous phase was extracted with DCM (2 × 20 mL). The organic phase was washed with water (20 mL) until the pH of the washing solution became neutral, dried ($MgSO_4$) and concentrated under reduced pressure, yielding an oil that was purified by silicagel (100–200 mesh) column chromatography using diethyl ether as the eluent. The desired compound crystallized at 4 °C after addition of diethyl ether. The ^1H and ^{13}C NMR spectra analyses showed that the purified compound was a single isomer, and C and H assignments were made on the basis of spin-spin decoupling, COSY, HSQC and HMBC experiments (data on Supporting Information). Furthermore, a long range correlation $^{TM}_C$ = 131.4 (C-5 pyrazole)/$^{TM}_H$ = 4.19 and 4.48 (N–CH_2–) in the HMBC spectrum clearly showed a 1,3-disubstituted pyrazole structure for the oxirane derivative **23**. Yield: 73%; mp: 53–55 °C; ^1H NMR ($CDCl_3$): δ 1.50–2.04 (m, 8H, $4CH_2$ cyclopent.), 2.53 (dd, J = 4.7, 2.6 Hz, 1H, H_A of CH_2 epox.), 2.85 (dd, J = 4.7, 4.3 Hz, 1H, H_B of CH_2 epox.), 3.34–3.40 (m, 1H, CHO epox.), 3.86 (s, 3H, OCH_3), 4.19 (dd, J = 4.6, 5.6 Hz, 1H, H_A of CH_2), 4.48 (dd, J = 14.6, 3.1 Hz, 1H, H_B of CH_2), 4.84–4.94 (m, 1H, OCH cyclopent.), 6.49 (d, J = 2.4 Hz, 1H, H-4 pyraz.), 6.88 (d, J = 8.3 Hz, 1H, H-5 Ar), 7,29 (dd, J = 8.3, 2.0 Hz, 1H, H-6 Ar), 7.36 (d, J = 2.0 Hz, 1H, H-2 Ar), 7.46 (d, J = 2.4 Hz, 1H, H-5 pyraz.); ^{13}C NMR ($CDCl_3$): 24.2 ($2CH_2$ cyclopent.), 32.9 ($2CH_2$ cyclopent.), 45.5 ($2CH_2$ cyclopent. epox.), 50.8 (CH epox.), 53.8 (CH_2N), 56.1 (OCH_3), 80.5 (OCH cyclopent.), 103.0 (C-4 pyraz.), 112.0 (C-5 Ar), 112.7 (C-2 Ar), 118.3 (C-6 Ar), 126.5 (C-1 Ar), 131.4 (C-5 pyraz.), 147.8 (C-3 Ar), 150.0 (C-4 Ar), 151.8 (C-3 pyraz.); Anal. ($C_{18}H_{22}N_2O_3$) calcd for C, H, N.

4.1.17. General procedure for the synthesis of 3-[3-(cyclopentyloxy)-4-methoxyphenyl]-1H-pyrazol-1-yl]-3-cycloaminopropan-2-ols ***8a,b***

An excess of the appropriate amine (2 mL) was added to 3-[3-(cyclopentyloxy)-4-methoxyphenyl]-1-(oxiran-2-ylmethyl)-1*H*-pyrazole **23** (1 g, 3.15 mmol) and the mixture was heated at 50–60 °C for 18 h. After cooling to room temperature, the mixture was diluted with diethyl ether (20 mL) and the organic phase was washed with water (20 mL), dried ($MgSO_4$) and concentrated under reduced pressure. The crude was purified by Florisil (100–200 mesh) column chromatography using diethyl ether as the eluent. The desired compounds were obtained as yellow oils that were treated with a HCl saturated ethanol solution to obtain the corresponding hydrochloride salts as white solids.

*4.1.17.1. 1-{3-[3-(Cyclopentyloxy)-4-methoxyphenyl]-1H-pyrazol-1-yl}-3-morpholin-4-ylpropan-2-ol dihydrochloride (****8a****).* Yield: 51%; mp: 162–163 °C; ^1H NMR ($CDCl_3$): δ 1.70–2.40 (m, 8H, $4CH_2$ cyclopent.), 3.20–3.60, 3.74–4.00, 4.10–4.25 and 4.25–4.50 (4 m, 10H, $4CH_2$ morph. + CH_2N), 4.05 (s, 3H, OCH_3), 4.80–5.35 (m, 5H, OCH cyclopent. + *CH*OH + CH_2N pyraz. + OH, 1H disappears with D_2O), 6.85 (br s, 1H, H-4 pyraz.), 7.09 (d, J = 8.2 Hz, 1H, H-5 Ar), 7.60 (d, J = 8.2 Hz, 1H, H-6 Ar), 7.75 (s, 1H, H-2 Ar), 8.24 (s, 1H, H-5 pyraz.), 11.70–11.95 (br s, 1H, NH^+ disappears with D_2O); IR (KBr): cm^{-1} 3550, 3150 (OH); Anal. ($C_{22}H_{31}N_3O_4.2HCl.2H_2O$) calcd for C, H, N.

4.1.18. Synthesis of 1-(3-{3-[3-(cyclopentyloxy)-4-methoxyphenyl]-1H-pyrazol-1-yl}-2-hydroxypropyl)piperidin-4-ol ***8c***

Piperidin-4-ol (0.25 g, 2.5 mmol) was added to a solution of 3-[3-(cyclopentyloxy)-4-methoxyphenyl]-1-(oxiran-2-ylmethyl)-1*H*-pyrazole **23** (0.38 g, 1.21 mmol) in anhydrous DMF (2 mL). The mixture was stirred at 50–60 °C for 18 h. After cooling to room temperature, the solvent was removed under reduced pressure. The residue was dissolved in diethyl ether (20 mL) and the organic phase was washed with water (20 mL), dried (Na_2SO_4), and concentrated under reduced pressure. The crude was purified by silicagel (100–200 mesh) column chromatography using as eluent first a mixture of diethyl ether/methanol (9:1) and then a mixture of DCM/methanol (7:3), obtaining the pure product as a light yellow oil. Yield: 40%, ^1H NMR ($CDCl_3$): δ 1.30–2.03 (m, 12H, $4CH_2$ cyclopent. + $2CH_2$ pip.), 2.03–2.99 (m, 8H, $3CH_2N$ + 2OH, 2H disappear with D_2O), 3.60–3.80 (m, 1H, *CH*–OH pip.), 3.88 (s, 3H, OCH_3), 4.04–4.28 (m, 3H, CH_2N pyraz. + *CH*OH), 4.78–4.98 (m, 1H, OCH cyclopent.), 6.49 (d, J = 2 Hz, 1H, H-4 pyraz.), 6.82–7.48 (m, 3H, H-6 + H-5 + H-2 Ar), 7.52 (d, J = 2.0 Hz, 1H, H-5 pyraz.); IR (KBr) cm^{-1}: 3413 (OH); Anal. ($C_{23}H_{33}N_3O_4$) calcd for C, H, N.

4.1.19. Synthesis of 2-{3-[3-(cyclopentyloxy)-4-methoxyphenyl]-1H-pyrazol-1-yl}-1-(morpholin-4-ylmethyl)ethyl acetate ***9a***

A mixture of 1-{3-[3-(cyclopentyloxy)-4-methoxyphenyl]-1*H*-pyrazol-1-yl}-3-morpholin-4-ylpropan-2-ol **8a** (0.60 g, 1.63 mmol) and sodium acetate (0.2 g, 2.4 mmol) in acetic anhydride (5 mL) was heated at 40–50 °C for 5 h. After cooling to room temperature, the mixture was poured into water (100 mL), extracted with diethyl ether (3 × 10 mL) and the organic phase was washed with water (3 × 20 mL), brine (3 × 20 mL), dried ($MgSO_4$) and concentrated under reduced pressure. The pure product was obtained as a yellow oil. Yield: 52%; ^1H NMR ($CDCl_3$): δ 1.56–2.06 (m, 8H, $4CH_2$ cyclopent.), 2.12 (s, 3H, CH_3), 2.61–2.92 (m, 6H, $2CH_2N$ morph. + CH_2N), 3.70–4.00 (m, 7H, OCH_3 + $2CH_2O$ morph.), 4.32–4.58 (m, 2H, CH_2N pyraz.), 4.81–4.99 (m, 1H, OCH cyclopent.), 5.40–5.57 (m, 1H, CHOAc), 6.50 (d, J = 1.6 Hz, 1H, H-4 pyraz.), 6.84–7.60 (m, 4H, H-6 + H-5 + H-2 Ar + H-5 pyraz.); IR (KBr) cm^{-1}: 1715 (CO); Anal. ($C_{24}H_{33}N_3O_5$) calcd for C, H, N.

4.1.20. General procedure for the synthesis of 4-(2-{3-[3-(cyclopentyloxy)-4-methoxyphenyl]-1H-pyrazol-1-yl}acetyl)amines ***10a,b***

The suitable chloroacetylamine (15 mmol) was added to a solution of 3-[3-(cyclopentyloxy)-4-methoxyphenyl]-1*H*-pyrazole **22** (0.52 g, 2 mmol) in an. DMF (3 mL). Then, TEA (1 mL, 0.73 g, 7.19 mmol) was added dropwise and the mixture was heated at 100 °C for 18 h. After cooling to room temperature, the mixture was poured into water (100 mL) and extracted with diethyl ether (3 × 25 mL). The organic phase was dried ($MgSO_4$) and concentrated under reduced pressure. The crude crystallized by addition of a mixture of diethyl ether/petroleum ether (boiling point 40–60 °C) (1:1) and the desired compounds were obtained as white solids, which were recrystallized by absolute ethanol (**10a**) or diethyl ether (**10b**).

*4.1.20.1. 4-(2-{3-[3-(cyclopentyloxy)-4-methoxyphenyl]-1H-pyrazol-1-yl}acetyl)morpholine (****10a****).* Yield: 58%; mp: 131–132 °C; ^1H NMR ($CDCl_3$): δ 1.60–2.12 (m, 8H, $4CH_2$ cyclopent.), 3.60–4.00 (m, 11H, OCH_3 + $4CH_2$ morph.), 4.83–5.10 (m, 3H, CH_2CO + OCH cyclopent.), 6.76 (d, J = 2.8 Hz, 1H, H-4 pyraz.), 6.96 (d, J = 8.2 Hz, 1H, H-5 Ar), 7.47 (dd, J = 8.2, 1.6 Hz, 1H, H-6 Ar), 7.68 (d, J = 1.6 Hz, 1H, H-2 Ar), 7.84 (d, J = 2.8 Hz, 1H, H-5 pyraz.); IR (KBr) cm^{-1}: 1663 (CO); Anal. ($C_{21}H_{27}N_3O_4$) calcd for C, H, N.

*4.1.21. Synthesis of 4-(3-{3-[3-(cyclopentyloxy)-4-methoxyphenyl]-1H-pyrazol-1-yl}propanoyl)morpholine **11a***

4-(3-chloropropanoyl)morpholine (3.20 g, 18 mmol), solved in anhydrous DMF (6 mL), was slowly added at 0 °C to a solution of 3-[3-(cyclopentyloxy)-4-methoxyphenyl]-1*H*-pyrazole **22** (0.77 g, 3 mmol) in anhydrous DMF (5 mL). Then, TEA (0.80 g, 7.91 mmol, 1.1 mL) was added dropwise and the mixture was heated at 120 °C for 48 h. After cooling to room temperature, the mixture was poured into water (100 mL), extracted with diethyl ether (3 × 25 mL) and the organic phase was dried ($MgSO_4$) and concentrated under reduced pressure. The crude was purified by silicagel (100–200 mesh) column chromatography using a gradient elution from diethyl ether to diethyl ether/methanol (1:1). The pure product was obtained as a light yellow oil. Yield: 38%; ^{1}H NMR ($CDCl_3$): δ 1.54–2.07 (m, 8H, $4CH_2$ cyclopent.), 2.91–3.00 (m, 2H, CH_2CO), 3.32–3.67 (m, 8H, $4CH_2$ morph.), 3.89 (s, 3H, OCH_3), 4.52 (t, *J* = 6.4 Hz, 2H, CH_2N), 4.89–5.00 (m, 1H, OCH cyclopent.), 6.44 (d, *J* = 2.4 Hz, 1H, H-4 pyraz.), 6.92 (d, *J* = 8.2 Hz, 1H, H-5 Ar), 7.22–7.40 (m, 2H, H-6 + H-2 Ar), 7.49 (d, *J* = 2.4 Hz, 1H, H-5 pyraz.); IR (film) cm^{-1}: 1654 (CO); Anal. ($C_{22}H_{29}N_3O_4$) calcd for C, H, N.

*4.1.22. Synthesis of methyl 3-{3-[3-(cyclopentyloxy)-4-methoxyphenyl]-1H-pyrazol-1-yl}-propanoate **24***

Methyl-3-bromopropionate (1.91 g, 11.45 mmol) and TEA (1 mL, 0.73 g, 7.19 mmol) were added dropwise at 0 °C to a solution of 3-[3-(cyclopentyloxy)-4-methoxyphenyl]-1*H*-pyrazole **22** (0.6 g, 2.25 mmol) in an. acetonitrile (15 mL); then, the mixture was heated at reflux for 48 h. After cooling to room temperature, the solvent was removed under reduced pressure and the crude was solved in diethyl ether (30 mL). The organic phase was washed with water (3 × 20 mL), 4 N NaOH solution (2 × 20 mL), brine (2 × 20 mL), dried ($MgSO_4$), and concentrated under reduced pressure. The obtained oil was purified by silicagel (100–200 mesh) column chromatography, using diethyl ether as the eluent to afford the pure product as a light yellow oil. Yield: 67%, ^{1}H NMR ($CDCl_3$): δ 1.50–2.18 (m, 8H, $4CH_2$ cyclopent.), 3.00 (t, *J* = 6.0 Hz, 2H, CH_2CO), 3.73 (s, 3H, OCH_3), 3.90 (s, 3H, OCH_3-Ar), 4.49 (t, *J* = 6.0 Hz, 2H, CH_2N), 4.77–5.08 (m, 1H, OCH cyclopent.), 6.45 (d, *J* = 3.0 Hz, 1H, H-4 pyraz.), 6.95 (d, *J* = 6.8 Hz, 1H, H-5 Ar), 7.20–7.50 (m, 3H, H-6 + H-2 Ar + H-5 pyraz.); IR ($CHCl_3$) cm^{-1}: 1735 (CO); Anal. ($C_{19}H_{24}N_2O_4$) calcd for C, H, N.

*4.1.23. Synthesis of 3-{3-[3-(cyclopentyloxy)-4-methoxyphenyl]-1H-pyrazol-1-yl}-propanoic acid **25***

NaOH (0.2 g, 5.0 mmol) was added to a solution of methyl 3-{3-[3-(cyclopentyloxy)-4-methoxyphenyl]-1*H*-pyrazol-1-yl}-propanoate **24** (1 g, 3 mmol) in 96% ethanol (3 mL) and the mixture was heated at 60 °C for 4 h. Then, the solvent was removed under reduced pressure, the crude was solved in water (20 mL) and a 1 N HCl solution was slowly added until pH became = 1. The light yellow solid obtained was filtered, washed with water and recrystallized by a mixture of diethyl ether/dichloromethane (1:1). Yield: 74%; mp: 131–133 °C; ^{1}H NMR ($CDCl_3$): δ 1.52–2.11 (m, 8H, $4CH_2$ cyclopent.), 3.02–3.10 (m, 2H, CH_2), 3.91 (s, 3H, OCH_3), 4.42–4.54 (m, 2H, CH_2N), 4.86–5.02 (m, 1H, OCH cyclopent.), 6.54 (d, *J* = 2.3 Hz, 1H, H-4 pyraz.), 6.93 (d, *J* = 8.4 Hz, 1H, H-5 Ar), 7.21–7.41 (m, 2H, H-6 + H-2 Ar), 7.52 (d, *J* = 2.3 Hz, 1H, H-5 pyraz.); IR ($CHCl_3$) cm^{-1}: 3515 (OH), 1721 (CO); Anal. ($C_{18}H_{22}N_2O_4$) calcd for C, H, N.

*4.1.24. Synthesis of 4-(3-{3-[3-(cyclopentyloxy)-4-methoxyphenyl]-1H-pyrazol-1-yl}propanoyl)2,6-dimethylmorpholine **11b***

TEA (0.30 g, 6 mmol, 0.4 mL), 2,6-dimethylmorpholine (0.50 mL, 4 mmol) and DPPA (0.69 g, 2.5 mmol) were added at 0 °C to a solution of 3-{3-[3-(cyclopentyloxy)-4-methoxyphenyl]-1*H*-pyrazol-1-yl}-propanoic acid **25** (0.67 g, 2 mmol) in anhydrous DMF (5 mL),. Then, the mixture was heated at 80 °C for 15 h. After cooling to room temperature, the mixture was poured into water (100 mL), extracted with diethyl ether (3 × 25 mL) and the organic phase was dried ($MgSO_4$) and concentrated under reduced pressure. The crude was purified by silicagel (100–200 mesh) column chromatography using diethyl ether as the eluent to afford the pure product as a light yellow oil. Yield: 71%; ^{1}H NMR ($CDCl_3$): δ 1.08 (d, *J* = 6.2 Hz, 3H, CH_3 morph), 1.18 (d, *J* = 6.2 Hz, 3H, CH_3 morph.), 1.60–2.06 (m, 8H, $4CH_2$ cyclopent.), 2.23–2.39, 2.62–2.7, 2.82–3.19 and 3.23–3.70 (4 m, 8H, $2CH_2$ morph. + CH_2CO + 2CH morph.), 3.89 (s, 3H, OCH_3), 4.50–4.59 (m, 2H, CH_2N), 4.86–4.97 (m, 1H, CHO cyclopent.), 6.43 (d, *J* = 2.2 Hz, 1H, H-4 pyraz.), 6.93 (d, *J* = 8.4 Hz, 1H, H-5 Ar), 7.33–7.41 (m, 2H, H-2 + H-6 Ar), 7.48 (d, *J* = 2.2 Hz, 1H, H-5 pyraz.); IR ($CHCl_3$) cm^{-1}: 1671 (CO); Anal. ($C_{24}H_{33}N_3O_4$) calcd for C, H, N.

4.2. Computational studies methods

4.2.1. Molecular dynamics and docking

Compounds **4a** and **8a** were built, parameterized (Gasteiger-Hückel method) and energy minimized within OpenEye Scientific Software [49] using MMFF94s force field. Regarding the protein, according to our previous studies, 1XOQ [50] was selected. For all calculations, only one molecular chain (chain A) was kept and hydrogen atoms were added at a neutral pH. The six waters into the catalytic site were maintained. Docking studies were performed using AutoDock 4.0 [51]. Molecular dynamics simulations of the complex PDE4D-inhibitor were performed using AMBER12 package [52], starting the experiments from the docking solutions in order to assess their stability along the trajectories. The ligands were parameterized using the semiempirical quantum chemistry method AM1-BCC to derive partial charges, while the other constants were derived by the Antechamber module for the GAFF force field [53,54]. The protein was parametrized with the AMBER ff03 force field. Mg^{2+} and Zn^{2+} ions were treated according to the "non-bonded" model method [55]. In order to remove all the possible bad contacts between atoms, preliminary minimization in vacuum of the system was run, using a steepest descendent algorithm until energy convergence of 0.0001 kcal/mol. The inhibitor-protein complex was solvated in a truncated octahedral periodic box with 8 Å of perimetral solvent thickness using TIP3P water model. Na^+ ions were added to neutralize the whole system. The simulations were performed at neutral pH, with histidines 164 and 200 protonated at delta position to coordinate the Zn^{2+} ion. The water molecule between the two ions was treated as hydroxide ion as suggested by studies of Li et al. [56] and by MD simulations studies on PDE11 previously performed [57]. Since HIS 160, close to the hydroxide ion, can readily capture a proton, it was protonated at both delta and epsilon positions. All the bonds involving hydrogen atoms were constrained by the SHAKE algorithm [58] and the time step was set to 2 fs. The non-bonded cut-off distance was 8 Å and long range electrostatic interactions were calculated using the Particle Mesh Ewald (PME) method. Four steps of minimization were performed, keeping the position of protein and ligand restrained for four minimization steps by a force constant of 500 kcal/mol/Å^2, 100 kcal/mol/Å^2 in the second, 10 kcal/mol/Å^2 in the third and without ligand and protein restrained in the fourth. All the minimization steps were run till the system energy convergence of 0.0001 kcal/mol was achieved. Next, the system was heated from 0 to 100 K in 30 ps, using Langevin dynamics at constant volume, and from 100 to 300 K in 20 ps at constant pressure. After that, the system was equilibrated for 7 ns at constant pressure of 1 atm. Position restrains of 10 kcal/mol/Å were used on

the ligand and protein during heating and equilibration steps. After equilibration, production molecular dynamics phase was performed at 300 K using constant pressure of 1 atm. The exploited method was validated performing a 20 ns MD simulation of the complex 1XOQ-Roflumilast. Then 70 ns MD run were performed for the docking complexes. The resulting trajectories were analysed using Amber Tools and VMD programs. The root mean square deviation (RMSD) was calculated for the protein backbone and ligand atoms using least-squares fitting. The pmemd CUDA program of the AMBER12 package was used for MD simulations running on a cluster Tesla K20 Graphical Processing Unit (GPU).

4.2.2. In silico evaluation of pharmacokinetic properties

The prediction of ADMET properties was performed using the Advanced Chemistry Development (ACD) Percepta platform (www.acdlabs.com).

Any pharmacokinetic and metabolism descriptor was evaluated by Percepta on the basis of training libraries, implemented in the software, which include a consistent number of molecules whose pharmacokinetic and toxicity profile are experimentally known.

4.3. Cytotoxicity and genotoxicity assays

The cells used in this study (human neuroblastoma cell line HTLA-230, HTLA) were grown in Roswell Park Memorial Institute medium (RPMI), with 0.1 mM non-essential aminoacids and 10% fetal bovine serum.

For the cytotoxicity assay, cells were treated for 24 h with 100 μM of the different compounds dissolved in DMSO. Control cells received the same volume of solvent (1 μL/ml medium). At the end of the incubation period, conditioned media were analysed for lactate-dehydrogenase release using the Cytoxicity Detection Kit-^{PLUS} (Roche, Germany), according to manufacturer protocols.

To evaluate genotoxicity, HTLA cells were treated for 24 h with the different compounds dissolved in DMSO and then processed for total protein extraction as described previously [59]. Immunoblots were done according to standard methods, using the following antibodies: mouse monoclonal [2F3] to gamma H2A.X (phospho S139) and rabbit polyclonal to Histone H2A.X (Abcam, UK); anti-mouse and anti-rabbit secondary antibodies coupled to horseradish peroxidase (GE Healthcare, UK). Proteins were visualized with an enzyme-linked chemiluminescence detection kit according to the manufacturer's instructions (GE Healthcare). Chemiluminescence was monitored by exposure to films and signals were analysed under non-saturating condition with an image densitometer (Bio-Rad, CA, USA).

4.4. cAMP enzymatic immunoassay (EIA)

Quantification of intracellular cAMP was performed with DetectX® Direct Cyclic AMP Enzyme Immunoassay Kit (Arbor Assay, MI, USA), following the manufacturer's protocol. cAMP levels were calculated according to the standard curves prepared on the same EIA plates.

4.5. Pharmacokinetic analysis

The pharmacokinetic analysis for **8a** and **11b** has been carried out by the Center for Drug Metabolism and Pharmacokinetics Research, Shanghai Institute of Materia Medica (Zhangjiang Hi-Tech Park, Pudong, Shanghai, China).

Detailed description of experimental procedure is reported online as supporting information material.

4.6. Microdialysis experiments

4.6.1. Animals

For the in vivo studies performed at Genoa University, all the experimental procedures were approved by the Italian Ministry of Health (protocol no. 29823) and were in accordance with the European (2010/63/UE) and Italian (D.L. 26/2014) guidelines on the use and care of laboratory animals.

4.6.2. Surgery and cAMP determination

Male Sprague-Dawley rats (250–300 g) were anaesthetized with intraperitoneal zoletil (tiletamine and zolazepam, 30 mg/kg), placed in a stereotaxic frame (David Kopf Instruments, West Hempstead, NY, USA) and implanted with microdialysis probes into the dorsal hippocampi according to the following coordinates: AP = +3.8, H = +6.5 from the interaural line (Paxinos and Watson atlas, 1986). A piece of dialysis fibre (co-polymer of acrylonitrile sodium methallyl sulphonate; AN69HF Hospal S.p.A., Bologna, Italy; 0.3 mm outer diameter, 40 kDa mol. wt. cut-off) was covered with epoxy glue to limit dialysis to the area of interest (8 mm glue-free length). The skull was exposed and two holes were drilled on the lateral surfaces. The dialysis probe was inserted transversely into the brain so that the glue-free zone was exactly positioned into the target area. Stainless steel cannulae (22-gauge diameter, 15-mm long) were glued to the ends of the fibre, bent up and fixed to the skull surface with dental cement and modified Eppendorf tips. After a 24-h recovery period, freely-moving rats were placed into observation cages and the probes infused with modified Ringer's medium (flow rate 5 μl/min; CMA/100 microinjection pump, CMA Microdialysis, Stockholm, Sweden) containing (in mM): NaCl 145, KCl 3, $MgCl_2$ 1, $CaCl_2$ 1.26, buffered at pH 7.4 with 2 mM phosphate buffer. Following a stabilization period of 1 h, consecutive samples were collected every 20 min. Compound **8a** was locally administered through the dialysis probe (retrodialysis) after three control samples had been collected to estimate cAMP basal values and was present in the infusion solution for the time reported in Fig. 7. At the end of the experiment, the correct position of the probe was verified by optical examination of the fibre tract. Animals presenting hemorrhagic lesions were rejected.

cAMP content in the dialysates was assayed by a commercially available radioimmunoassay kit (IZOTOP, Institute of isotopes, Co., Ltd., Budapest, Hungary) using the acetylation protocol. Under these experimental conditions, the detection limit of the assay is 2 fmol (standard curve range 2–128 fmol).

4.7. Behavioral studies

4.7.1. Animals

For the studies performed at Maastricht University, the experimental procedures were approved by the local ethics committee of Maastricht University for animal experiments and met governmental guidelines. For the **8a** study, twenty-four male Wistar rats were supplied by Charles River (Sulzfeld. Germany) and tested between 4 and 5 months of age. Average body weight at the beginning of the study was 436 g. All animals were housed individually in standard green line Techiplast IVC cages on sawdust bedding. The animals were housed on a reversed 12/12-h light/dark cycle (lights on from 19:00 h to 07:00 h) and had free access to food and water. The rats were housed and tested in the same room. A radio, playing softly, provided background noise in the room. Testing was performed between 09:00 h and 18:00 h, with a small desk lamp providing light for the experimenter.

4.7.2. Treatments

8a and scopolamine were both dissolved in saline. Vehicle or

doses of 0.001, 0.003 and 0.01 mg/kg **8a** were given intraperitoneal (IP) at an injection volume of 1 mL/kg, 3 h after the first trial with the 24 h inter-trial interval ORT. For the 1 h inter-trial interval ORT with a scopolamine induced memory deficit, vehicle or scopolamine (0.1 mg/kg IP) were administered 30 min before the start of the first trial. **8a** was tested at doses of 0.001, 0.003 and 0.01 mg/kg (IP), administered 30 min before the first trial. Doses of, 0.003, 0.03 and 0.3 mg/kg of **8a** were tested in the xylazine (10 mg/kg IP)/ketamine (10 mg/kg IP) induced α_2-adrenoceptor-mediated anaesthesia test. Vehicle or **8a** were administered subcutaneously (SC) 15 min after the xylazine/ketamine injections.

4.7.3. Object recognition task (rats)

The ORT has been performed as previously described elsewhere [41,44].

Detailed description of experiments is reported online as supporting information material.

4.7.4. Xylazine/ketamine induced α_2-adrenoceptor-mediated anaesthesia test

To investigate possible emetic-like effect of **8a** the rats were anaesthetized with an IP injection of 10 mg/kg ketamine and 10 mg/kg xylazine (injection volume of 1 mL/kg). 15 min after the induction of the anaesthesia, vehicle or one of the concentrations of **8a** solutions was administrated, after which the rats were put in dorsal position. The outcome measurement was the total time the animals were anaesthetized, measured from the induction of the anaesthesia to the righting reflex when the rats were back on all four paws. To get a sufficient group size, the experiments were repeated three times with 2 recovery days in between. The animals received the same condition only once.

4.8. Statistical analysis

4.8.1. In vitro cAMP evaluation

Data presented (mean ± S.E.M) are expressed as pmol/ml. Differences were analysed by ANOVA followed by multiple comparison Dunnett's test. Differences were considered significant at the level of $p < 0.05$, at least.

4.8.2. In vivo cAMP evaluation

Data presented (mean ± S.E.M) are expressed as percentages of the mean basal value (defined as 100%) that was determined by averaging the content of the first 3 samples collected before drug treatment. Differences were analysed by ANOVA followed by Bonferroni's post hoc comparison test. Differences were considered significant at the level of $p < 0.05$, at least.

4.8.3. ORT

The readout parameters of the ORT are the times that rodents spent on exploring each object during T1 and T2 [42,60]. The exploration time (in seconds) of each object during T1 is presented as 'a1' and 'a2'. The time spent exploring the familiar and the novel object in T2 is represented as 'a3' and 'b', respectively. Using this information, the following variables were calculated: e1, e2 and d2 (see Table below). The d2 index is a relative measure of discrimination corrected for exploratory activity and it has been shown not to be correlated to e1 or e2 [60]. The d2 index can range from −1 to 1. A significant difference from zero indicates that the rats remembered the object from T1, and a difference from the vehicle condition signifies an actual memory improvement. Of note, rats require a minimum amount of exploration in order to show reliable memory performance [41,42]. Therefore, animals were removed from the analysis if they spent less than 9 s exploring the objects during T1 or T2. One sample t-tests were used to compare the d2 index of the conditions to zero (i.e. chance level). However, comparison of the d2 value with the value zero with no variance is not the most suitable way of analysing object recognition since there is an increased chance of making a type I error. For this reason, a one-way ANOVA was performed to find significant differences between d2 values of the conditions. When significant, post-hoc Dunnett's t-tests were performed to compare the experimental conditions to the vehicle group.

Trial	Exploration time (s)	Discrimination index
T1	e1 = a1 + a2	–
T2	e2 = a3 + b	d2 = (b − a3)/e2

4.8.4. Xylazine/ketamine induced α_2-adrenoceptor-mediated anaesthesia test

Total time of anaesthesia was used as an outcome measurement. To control for the differences between test days, the vehicle condition was set to 100% and the times of the **8a** conditions were expressed in relation to this. To test for statistical significance between conditions, a one-way ANOVA was performed with these relative times. When significant, post-hoc Dunnett's t-tests were performed to compare the experimental conditions to the vehicle condition.

Conflict of interest

OB, CB, AR, EF, RR, OA, JP have a proprietary interest in selective PDE4D inhibitors, including **8a**.

Authors contributions

CB, OB: molecules design and SAR; MM, CR, AR: molecules synthesis, purification and characterization; JP, BTJvH, NPvG: behavior studies; OA: pharmacokinetic analysis; RR, EF, CR, BM, MAP: cyto- and genotoxic tests; in vitro and in vivo cAMP measures; EC, PF, SG, PdU, AO, LM: in silico physico-chemical properties evaluation, docking studies and molecular dynamics simulation.

OB, CB, PF, RR, EF, OA, JP wrote the article.

Acknowledgements

Alzheimer Association is gratefully acknowledged for financial support to this study (IIRG 11-208306). We thank Dr. M. Anzaldi, R. Raggio, Mr. O. Gagliardo, and F. Tuberoni for spectral recording and Mr. V. Ruocco for the informatics support to calculations.

B.T.J. van Hagen is financially supported by the Human Enhancement and Learning (HEaL) initiative of Maastricht University. This work has been supported by the Italian Ministry of Education and Research through the Flagship "InterOmics" (PB05) and European MIMOmics (305280) Projects.

Appendix A. Supplementary data

Supplementary data related to this article can be found at http://dx.doi.org/10.1016/j.ejmech.2016.08.018.

References

[1] R. Bourtchuladze, B. Frenguelli, J. Blendy, D. Cioffi, G. Schutz, A.J. Silva, Deficient long-term memory in mice with a targeted mutation of the cAMP-responsive element-binding protein, Cell 79 (1994) 59–68.

[2] J.C.P. Yin, J.S. Wallach, M. Del Vecchio, E.L. Wilder, H. Zhou, W.G. Quinn,

T. Tully, Induction of a dominant negative CREB transgene specifically blocks long-term memory in Drosophila, Cell 79 (1994) 49–58.
[3] O.V. Vitolo, A. Sant'Angelo, V. Costanzo, F. Battaglia, O. Arancio, M. Shelanski, Amyloid beta -peptide inhibition of the PKA/CREB pathway and long-term potentiation: reversibility by drugs that enhance cAMP signaling, Proc. Natl. Acad. Sci. U. S. A. 99 (2002) 13217–13221.
[4] B. Gong, O.V. Vitolo, F. Trinchese, S. Liu, M. Shelanski, O. Arancio, Persistent improvement in synaptic and cognitive functions in an Alzheimer mouse model after rolipram treatment, J. Clin. Investig. 114 (2004) 1624–1634.
[5] A.F. Teich, R.E. Nicholls, D. Puzzo, J. Fiorito, R. Purgatorio, M. Fa', O. Arancio, Synaptic therapy in Alzheimer's disease: a CREB-centric approach, Neurotherapeutics 12 (2015) 29–41.
[6] M.E. Gurney, E.C. D'Amato, A.B. Burgin, Phosphodiesterase-4 (PDE4) molecular pharmacology and Alzheimer's disease, Neurotherapeutics 12 (2015) 49–56.
[7] M. Barad, R. Bourtchouladze, D.G. Winder, H. Golan, E. Kandel, Rolipram, a type IV-specific phosphodiesterase inhibitor, facilitates the establishment of long-lasting long-term potentiation and improves memory, Proc. Natl. Acad. Sci. U. S. A. 95 (1998) 15020–15025.
[8] R. Bourtchouladze, R. Lidge, R. Catapano, J. Stanley, S. Gossweiler, D. Romashko, R. Scott, T. Tully, A mouse model of Rubinstein-Taybi syndrome: defective long-term memory is ameliorated by inhibitors of phosphodiesterase 4, Proc. Natl. Acad. Sci. U. S. A. 100 (2003) 10518–10522.
[9] B. Gong, O.V. Vitolo, F. Trinchese, S. Liu, M. Shelanski, O. Arancio, Persistent improvement in synaptic and cognitive functions in an Alzheimer mouse model after rolipram treatment, J. Clin. Investig. 114 (2004) 1624–1634.
[10] C. Giampà, S. Middei, S. Patassini, A. Borreca, F. Marullo, D. Laurenti, Phosphodiesterase type IV inhibition prevents sequestration of CREB binding protein, protects striatal parvalbumin interneurons and rescues motor deficits in the R6/2 mouse model of Huntington's disease, Eur. J. Neurosci. 29 (2009) 902–910.
[11] O.A. Reneerkens, K. Rutten, H.W. Steinbusch, A. Blokland, J. Prickaerts, Selective phosphodiesterase inhibitors: a promising target for cognition enhancement, Psychopharmacol. Berl. 202 (2009) 419–443.
[12] A. Garcia-Osta, M. Cuadrado-Tejedor, C. Garcia-Barroso, J. Oyarzabal, R. Franco, Phosphodiesterases as therapeutic targets for Alzheimer's disease, ACS Chem. Neurosci. 3 (2012) 832–844.
[13] O. Bruno, E. Fedele, J. Prickaerts, L. Parker, E. Canepa, C. Brullo, A. Cavallero, E. Gardella, A. Balbi, C. Domenicotti, E. Bollen, H. Gijselaers, T. Vanmierlo, K. Erb, C. Limebeer, F. Argellati, U. Marinari, M. Pronzato, R. Ricciarelli, GEBR-7b, a novel PDE4D selective inhibitor that improves memory in rodents at non-emetic doses, Brit. J. Pharmacol. 164 (2011) 2054–2063.
[14] A.S.R. Sierksma, D.L.A. Van den Hove, F. Pfau, M. Philippens, O. Bruno, E. Fedele, R. Ricciarelli, H.W.M. Steinbusch, T. Vanmierlo, J. Prickaerts, Improvement of spatial memory function in APPswe/PS1dE9 mice after chronic inhibition of phosphodiesterase type 4D, Neuropharmacology 77 (2014) 120–130.
[15] A.B. Burgin, O.T. Magnusson, J. Singh, P. Witte, B.L. Staker, J.M. Bjornsson, M. Thorsteinsdottir, S. Hrafnsdottir, T. Hagen, A.S. Kiselyov, L.J. Stewart, M.E. Gurney, Design of phosphodiesterase 4D (PDE4D) allosteric modulators for enhancing cognition with improved safety, Nat. Biotechnol. 28 (2010) 63–70.
[16] Y.F. Li, Y.F. Cheng, Y. Huang, M. Conti, S.P. Wilson, J.M. O'Donnell, H.T. Zhang, Phosphodiesterase-4D knock-out and RNA interference-mediated knockdown enhance memory and increase hippocampal neurogenesis via increased cAMP signaling, J. Neurosci. 31 (2011) 172–183.
[17] M.D. Houslay, G.S. Baillie, D.H. Maurice, cAMP-Specific phosphodiesterase-4 enzymes in the cardiovascular system: a molecular toolbox for generating compartmentalized cAMP signaling, Circ. Res. 100 (2007) 950–966.
[18] M.D. Houslay, R.D. Adams, PDE4 cAMP phosphodiesterases: modular enzymes that orchestrate signalling cross-talk, desensitization and compartmentalization, Biochem. J. 370 (2003) 1–18.
[19] W. Richter, M. Conti, The oligomerization state determines regulatory properties and inhibitor sensitivity of type 4 cAMP-specific phosphodiesterases, J. Biol. Chem. 279 (2004) 30338–30348.
[20] W. Richter, M. Conti, Dimerization of type 4 cAMP-specific phosphodiesterases is mediated by the upstream conserved regions (UCRs), J. Biol. Chem. 277 (2002) 40212–40221.
[21] D. Fox, A.B. Burgin, M.E. Gurney, Structural basis for the design of selective phosphodiesterase 4B inhibitors, Cell. Signal. 26 (2014), 657–633.
[22] P. Cedervall, A. Aulabaugh, K.F. Geoghegan, T.J. McLellan, J. Pandit, Engineered stabilization and structural analysis of the autoinhibited conformation of PDE4, Proc. Natl. Acad. Sci. U. S. A. 112 (2015) E1414.
[23] J. Pandit, PDE4: new structural insights into the regulatory mechanism and implications for the design of selective inhibitors, in: S. Liras, A.S. Bell (Eds.), Phophodiesterases and Their Inhibitors, Wiley-VCH, 2014, pp. 29–40.
[24] P.H. Schafer, A. Parton, A.K. Gandhi, L. Capone, M. Adams, L. Wu, J.B. Bartlett, M.A. Loveland, A. Gilhar, Y.F. Cheung, G.S. Baillie, M.D. Houslay, H.W. Man, G.W. Muller, D.I. Stirling, Apremilast, a cAMP phosphodiesterase-4 inhibitor, demonstrates anti-inflammatory activity in vitro and in a model of psoriasis, Br. J. Pharmacol. 159 (2010) 842–855.
[25] D.S. Bundschuh, M. Eltze, J. Barsig, L. Wollin, A. Hatzelmann, R. Beume, In vivo efficacy in airway disease models of roflumilast, a novel orally active PDE4 inhibitor, J. Pharm. Exp. Ther. 297 (2001) 280–290.
[26] J.E. Souness, S. Rao, Proposal for pharmacologically distinct conformers of PDE4 cyclic AMP phosphodiesterases, Cell. Signal. 9 (1997) 227–236.
[27] J. Singh, M.E. Gurney. Preparation of substituted aza-bridged bicyclics as PDE4 inhibitors for treatment of cardiovascular and CNS disease and other disorders. WO2010059836A1 (2010).
[28] O. Bruno, C. Brullo, N. Arduino, S. Schenone, A. Ranise, F. Bondavalli, L. Ottonello, P. Dapino, F. Dallegri, Synthesis and biological evaluation of neutrophilic inflammation inhibitors, Il Farm. 59 (2004) 223–235.
[29] O. Bruno, A. Romussi, A. Spallarossa, C. Brullo, S. Schenone, F. Bondavalli, F.N. Vanthuyne, C. Roussel, New selective phosphodiesterase 4D inhibitors differently acting on long, short, and supershort isoforms, J. Med. Chem. 52 (2009) 6546–6557.
[30] C. Brullo, M. Massa, M. Rocca, C. Rotolo, S. Guariento, D. Rivera, R. Ricciarelli, E. Fedele, P. Fossa, O. Bruno, Synthesis, biological evaluation, and molecular modeling of new 3-(Cyclopentyloxy)-4-methoxybenzaldehyde O-(2-(2,6-Dimethylmorpholino)-2-oxoethyl) oxime (GEBR-7b) related phosphodiesterase 4D (PDE4D) inhibitors, J. Med. Chem. 57 (2014) 7061–7072.
[31] C. Brullo, M. Massa, C. Villa, R. Ricciarelli, D. Rivera, M.A. Pronzato, E. Fedele, E. Barocelli, S. Bertoni, L. Flammini, O. Bruno, Synthesis, biological activities and pharmacokinetic properties of new fluorinated derivatives of selective PDE4D inhibitors, Bioorg. Med. Chem. 23 (2015) 3426–3435.
[32] P. D'Ursi, S. Guariento, G. Trombetti, A. Orro, E. Cichero, L. Milanesi, P. Fossa, O. Bruno, Further insights in the binding mode of selective inhibitors to human PDE4D enzyme combining docking and molecular dynamics, Mol. Inf. (2016), http://dx.doi.org/10.1002/minf.201501033.
[33] M.J. Ashton, D.C. Cook, G. Fenton, J.A. Karlsson, M.N. Palfreyman, D. Raeburn, Selective type IV phosphodiesterase inhibitors as antiasthmatic agents. The synthesis and biological activities of 3-(cyclopentyloxy)-4-methoxybenzamides and analogues, J. Med. Chem. 37 (1994) 1696–1703.
[34] H.O.H. Kan, I. Adachi, R. Kido, K. Hirose, Isoxazoles. XVIII. Synthesis and pharmacological properties of 5-Aminoalkyl- and 3-Aminoalkylisoxazoles and related derivatives, J. Med. Chem. 10 (1967) 411–418.
[35] H. Kano, I. Adachi, R. Kido, K. Hirose, Isoxazoles. XVIII. Synthesis and pharmacological properties of 5-Aminoalkyl- and 3-Aminoalkylisosazoles and related derivatives, J. Med. Chem. 10 (1967) 411–418.
[36] V.K. Aggarwal, J. de Vicente, R.V. Bonnert, A novel one-pot method for the preparation of pyrazoles by 1,3-dipolar cycloadditions of diazo compounds generated in situ, J. Org. Chem. 68 (2003) 5381–5383.
[37] H. Waterbeemd, E. Gifford, ADMET in silico modelling: towards prediction paradise? Nat. Rev. Drug Discov. 2 (2003) 192–204.
[38] W.M. Bonner, C.E. Redon, J.S. Dickey, A.J. Nakamura, O.A. Sedelnikova, S. Solier, Y. Pommier, GammaH2AX and cancer, Nat. Rev. Cancer 8 (2008) 957–967.
[39] A. Montecucco, G. Biamonti, Cellular response to etoposide treatment, Cancer Lett. 252 (2007) 9–18.
[40] A. Ennaceur, J. Delacour, A new one-trial test for neurobiological studies of memory in rats. 1: behavioral data, Behav. Brain Res. 31 (1988) 47–59.
[41] J. Prickaerts, A. Sik, F.J. van der Staay, J. de Vente, A. Blokland, Dissociable effects of acetylcholinesterase inhibitors and phosphodiesterase type 5 inhibitors on object recognition memory: acquisition versus consolidation, Psychopharmacol. Berl. 177 (2005) 381–390.
[42] S. Akkerman, A. Blokland, O. Reneerkens, N.P. van Goethem, E. Bollen, H.J. Gijselaers, C.K. Lieben, H.W. Steinbusch, J. Prickaerts, Object recognition testing: methodological considerations on exploration and discrimination measures, Behav. Brain Res. 232 (2012) 335–347.
[43] A. Sik, P. van Nieuwehuyzen, J. Prickaerts, A. Blokland, Performance of different mouse strains in an object recognition task, Behav. Brain Res. 147 (2003) 49–54.
[44] K. Rutten, E.L. Van Donkelaar, L. Ferrington, A. Blokland, E. Bollen, H.W. Steinbusch, P.A. Kelly, J.H. Prickaerts, Phosphodiesterase inhibitors enhance object memory independent of cerebral blood flow and glucose utilization in rats, Neuropsychopharmacology 34 (2009) 1914–1925.
[45] A. Robichaud, C. Savoie, P.B. Stamatiou, N. Lachance, P. Jolicoeur, R. Rasori, C.C. Chan, Assessing the emetic potential of PDE4 inhibitors in rats, Brit. J. Pharmacol. 135 (2002) 113–118.
[46] T. Vanmierlo, P. Creemers, S. Akkerman, M. van Duinen, A. Sambeth, J. De Vry, T. Uz, A. Blokland, J. Prickaerts, The PDE4 inhibitor roflumilast improves memory in rodents at non-emetic doses, Behav. Brain Res. 303 (2016) 26–33.
[47] K. Rutten, J. Prickaerts, A. Blokland, Rolipram reverses scopolamine-induced and time-dependent memory deficits in object recognition by different mechanisms of action, Neurobiol. Learn. Mem. 85 (2006) 132–138.
[48] M.E. Gurney, A.B. Burgin, O.T. Magnusson, L.J. Stewart, Small molecule allosteric modulators of phosphodiesterase 4, Handb. Exp. Pharm. 204 (2011) 167–192.
[49] OpenEye Scientific Software, Santa Fe, New Mexico, USA http://www.eyesopen.com/www.eyesopen.com.
[50] G.L. Card, B.P. England, Y. Suzuki, D. Fong, B. Powell, B. Lee, C. Luu, M. Tabrizizad, S. Gillette, P.N. Ibrahim, D.R. Artis, G. Bollag, M.V. Milburn, S.H. Kim, J. Sclessinger, K.Y. Zhang, Structural basis for the activity of drugs that inhibit phosphodiesterases, Structure 12 (2004) 2233–2247.
[51] G.M. Morris, R. Huey, W. Lindstrom, M.F. Sanner, R.K. Belew, D.S. Goodsell, A. Olson, AutoDock4 and AutoDockTools4: automated docking with selective receptor flexibility, J. Comput. Chem. 16 (2009) 2785–2791.
[52] D.A. Case, T.A. Darden, T.E. Cheatham III, C.L. Simmerling, J. Wang, R.E. Duke, R. Luo, R.C. Walker, W. Zhang, K.M. Merz, B. Roberts, S. Hayik, A. Roitberg, G. Seabra, J. Swails, A.W. Goetz, I. Kolossvary, K.F. Wong, F. Paesani, J. Vanicek, R.M. Wolf, J. Liu, X. Wu, S.R. Brozell, T. Steinbrecher, H. Gohlke, Q. Cai, X. Ye, J. Wang, M.J. Hsieh, G. Cui, D.R. Roe, D.H. Mathews, M.G. Seetin, R. Salomon-

Ferrer, C. Sagui, V. Babin, T. Luchko, S. Gusarov, A. Kovalenko, P.A. Kollman, AMBER 12, University of California, San Francisco, 2012.
[53] A. Jakalian, D.B. Jack, C.I. Bayly, Fast, efficient generation of high-quality atomic charges. AM1-BCC model: II. Parameterization and validation, J. Comput. Chem. 23 (2002) 1623–1641.
[54] J. Wang, W. Wang, P.A. Kollman, D.A. Case, Development and testing of a general amber force field, J. Comput. Chem. 25 (2004) 1157–1174.
[55] R.H. Stote, M. Karplus, Zinc binding in proteins and solution: a simple but accurate nonbonded representation, Proteins 23 (1995) 12–31.
[56] Z. Li, Y.H. Cai, Y.K. Cheng, X. Lu, Y.X. Shao, X. Li, M. Liu, P. Liu, H.B. Luo, Identification of novel phosphodiesterase-4D inhibitors prescreened by molecular dynamics-augmented modeling and validated by bioassay, J. Chem. Inf. Model. 53 (2013) 972–981.
[57] E. Cichero, P. D'Ursi, M. Moscatelli, O. Bruno, A. Orro, C. Rotolo, L. Milanesi, P. Fossa, Homology modeling, docking studies and molecular dynamics simulations using graphical processing unit architecture to probe the type-11 phosphodiesterase catalytic site: a computational approach for the rational design of selective inhibitors, Chem. Biol. Drug Des. 82 (2013) 718–731.
[58] S. Miyamoto, P.A. Kollman, Settle: an analytical version of the SHAKE and RATTLE algorithm for rigid water models, J. Comput. Chem. 8 (1992) 952–962.
[59] C. d'Abramo, R. Ricciarelli, M.A. Pronzato, P. Davies, Troglitazone, a peroxisome proliferator-activated receptor-gamma agonist, decreases tau phosphorylation in CHOtau4R cells, J. Neurochem. 98 (2006) 1068–1077.
[60] S. Akkerman, J. Prickaerts, H.W. Steinbusch, A. Blokland, Object recognition testing: statistical considerations, Behav. Brain Res. 232 (2012) 317–322.